Descriptive osteology and patterns of limb loss of the European limbless skink *Ophiomorus punctatissimus* (Squamata, Scincidae)

Marco Camaiti[1,2], Andrea Villa[1,3], Lukardis C.M. Wencker[1], Aaron M. Bauer[4], Edward L. Stanley[5], Massimo Delfino[1,6]

[1]*Dipartimento di Scienze della Terra, Università di Torino, Turin, Italy*
[2]*School of Biological Sciences, Monash University, Clayton, VIC, Australia*
[3]*Bayerische Staatssammlung für Paläontologie und Geologie, München, Germany*
[4]*Department of Biology, Villanova University, Villanova, PA, USA*
[5]*Department of Herpetology, Florida Museum of Natural History, Gainesville, FL, USA*
[6]*Institut Català de Paleontologia Miquel Crusafont, Universitat Autònoma de Barcelona, Barcelona, Spain*

ABSTRACT

The limbless skink *Ophiomorus punctatissimus* is a cryptozoic species found in the Peloponnese region of Greece and on the Greek island Kythira. In order to provide a first thorough description of the cranial and postcranial osteology of this species, both disarticulated specimens and X-ray computed tomographies of wet-preserved specimens are herein examined in detail. Resulting from this, an anatomical atlas of this species is provided. Two separate considerations, an evolutionary and an ecomorphological one, are made based on the observed adaptations related to limb loss in this skink. The structure of the girdles shows a particular pattern of reduction: whereas the pelvic girdle is mostly vestigial, the pectoral girdle is instead well developed, with all the elements typical of limbed lizards except for the actual limbs. This led us to hypothesize an asynchronous pattern of limb reduction during the evolution of this species, in which the hindlimbs regressed earlier than the forelimbs. Furthermore, considerations based on overall body morphology, osteology and the structure of the inner ear led to the recognition of this species as a burrowing ecomorph. In contrast to the morphology normally displayed in this ecomorph, *Ophiomorus punctatissimus* is characterized by the retention of autotomic vertebrae in its tail. This is consistent with the habitats in which it lives, where active burrowing would be difficult because of the hard, rocky terrain. Instead, this skink hides among rocks on the surface and is, therefore, subject to greater predation risk.

KEYWORDS: lizards; reptiles; CT-scans; comparative anatomy; inner ear.

INTRODUCTION

The scincid lizard genus *Ophiomorus* was first described by Duméril and Bibron (1839) to accommodate the species *Ophiomorus miliaris* Duméril and Bibron 1839, intended as a "junior objective synonym of *Anguis punctatissimus*" (Anderson and Leviton, 1966: 500, 525), which was subsequently renamed as *Ophiomorus punctatissimus* (Boulenger, 1887). The genus *Ophiomorus* currently comprises 12 extant species (Kazemi et al., 2011; Kornilios et al., 2018), ranging from southeastern Europe (mainland of Greece) to western India (Anderson and Leviton, 1996). Following the first revision of the genus by Boulenger (1887), in which six species were recognized (*Ophiomorus blanfordi*, *O. brevipes*, *O. latastii*, *O. persicus*, *O. punctatissimus*, *O. tridactylus*),

three more were added by Anderson and Leviton (1966): *O. chernovi*, *O. raithmai* and *O. streeti*. The subsequent description of *O. nuchalis* Nilson and Andrén, 1978 and *Ophiomorus maranjabensis* Kazemi et al., 2011 raised that number to 11. In 2018, a twelfth species was described as *O. kardesi* Kornilios et al., 2018, to accommodate the Anatolian populations previously attributed to *O. punctatissimus* (Kornilios et al., 2018).

The members of this skink genus are characterized by a strong tendency towards limb reduction, ranging from species having short limbs and a reduced number of fingers to completely limbless species.

These skinks are cryptozoic, as they live in underground burrows or under rocks and are rarely seen in the open (Greer and Wilson, 2001). More specifically, the genus shows two main adaptations: the western species group (*O. latastii*, *O. persicus*, *O. punctatissimus*) displays the greatest degree of limb reduction and adaptation to a life under rocks, whereas the eastern species group (*O. blanfordi*, *O. brevipes*, *O. chernovi*, *O. raithmai*, *O. streeti*, *O. tridactylus*, *O. nuchalis*) dwells in sand dune environments and has less reduced limbs (Anderson and Leviton, 1966).

A cladistic analysis based on morphological data by Greer and Wilson (2001) supported the monophyly of the group as a whole. However, a rigid distinction between an eastern and a western group was only partially confirmed: the eastern species group was shown to be monophyletic, whereas the monophyly of the western species group remains uncertain. *Ophiomorus maranjabensis* and *O. kardesi*, which were described after the study of Greer and Wilson (2001) was conducted, were identified, respectively, as sister taxa of *O. raithmai* (thus suggesting inclusion in the eastern species group, in accordance with its geographic provenance) and of *O. punctatissimus* (Kazemi et al., 2011; Kornilios et al., 2018).

Ophiomorus punctatissimus (Bibron and Bory de St. Vincent, 1833) (Fig. 1) is the westernmost extant representative of its genus, and the only one occurring exclusively in Europe. It is found in the Peloponnese region (southeast mainland of Greece) and on the Greek island Kythira, from sea level to 800 m elevation (Hermann and Stadler, 2008; Poulakakis et al., 2008) (Fig. 2). Prior to the renaming of the Anatolian populations of *O. punctatissimus* as *O. kardesi* by Kornilios et al. (2018), southwestern Turkey was considered part of the disjunct areal of the former (Anderson and Leviton, 1966). *Ophiomorus punctatissimus* is normally found in plantations and temperate grasslands with sparse vegetation and scarce rainfall but can also be found in more vegetated and humid environments (Rödel et al., 1989; Lymberakis et al., 2009). Being a cryptozoic species, very little is known about the lifestyle of this skink. However, specimens of *O. punctatissimus* have been found predominantly under rocks and it is known to feed on small invertebrates and to be oviparous (Anderson and Leviton, 1966; Speybroeck et al., 2016). The species is listed as Least Concern (LC)

in the Red List of Threatened Species of the International Union for Conservation of Nature (IUCN) (Lymberakis et al., 2009).

This study aims to provide a more in-depth picture of this species, particularly regarding its osteology. Based on the latter, we tentatively further investigate the evolutionary history and adaptive significance of its limblessness.

Institutional abbreviations

MCCI: Museo Civico di Storia Naturale di Carmagnola, Italy.

MCZ: Museum of Comparative Zoology, Cambridge, Massachusetts, United States of America.

MDHC: Massimo Delfino Herpetological Collection, University of Torino, Italy.

Materials and methods

We studied five preserved specimens of *Ophiomorus punctatissimus*: two skeletonized specimens catalogued as MDHC 427 and MCZ 38517, and three specimens wet-preserved in 90% alcohol, labeled as MCCI R775, MCCI R776 and MCCI R0952. Some of the bones were not found in MDHC 427, probably either because of their lack of mineralization or because they were lost during preparation of the specimen. These bones are the palpebral, the stapes, the hyoid bones, the interclavicle, the sternum and all caudal vertebrae except for the anterior caudal vertebra and the first eight autotomic vertebrae. Nevertheless, it was still possible to obtain information about the morphology of these bones from the wet-preserved specimens. The tail of MDHC 427 was reported as regenerated, thus probably accounting for the lack of most parts of the caudal vertebrae. The SVL (snout-vent length) of this specimen prior to skeletonization was reported to be 47 mm, whereas its total length was of 110 mm, keeping in mind that its tail was regenerated.

The descriptions of the cranial region follow the terminology of Evans (2008), Gelnaw (2011), and Paluh and Bauer (2017). Identification and description of the postcranial bones were based on Russell and Bauer (2009). We followed Andrade et al. (2016) for the identification of the appendicular skeleton, and the vertebral elements were named according to Tschopp (2016). The descriptions of the single cranial bones are ordered according to Evans (2008).

The isolated bones were studied using an optical microscope and were photographed with a Leica M205 C microscope. Image stacking was applied with the Leica application suite software (V 4.10) to partially avoid limited depth focus. The three wet-preserved specimens of *O. punctatissimus* were CT-scanned at Microservice S.r.l. (Alpignano, TO) with a Nikon XTH320, and then their 3D inner skeletal structures were analyzed and rendered with the MyVGL 3.0, VGStudioMax 3.2.2 and

Zbrush 4R8 software. The original resolution of the CT scans was of 13.187130 µm in the case of the head-only scans of all three specimens and of 42.357540 µm in the case of the full body scan of MCCI R776. The TIFF image stack of each scan consisted of 3601 slices.

The few differences recognized between the CT-scanned and the skeletonized specimens most likely originate from artefacts due to insufficient resolution in the scanning. This is explicitly stated in the descriptions, when necessary.

Osteoderms are not described in this article. The very small size and, above all, thinness, of the composite osteoderms of *O. punctatissimus* requires appropriate CT scans that will be performed in the frame of another project dealing specifically with the intra- and interspecific variation of osteoderms in skinks.

Specimen localities

MDCH 427: unknown locality, Peloponnese, Greece.

MCZ 38517: Corinth, Peloponnese (Corinthia), Greece.

MCCI R0775: Xirocambia-Pelopanagia (between), Peloponnese (Laconia), Greece.

MCCI R0776: Acrokorinthos, Peloponnese (Corinthia), Greece.

MCCI R0952: Leonidio-Paleohori, Peloponnese (Arcadia), Greece.

RESULTS

Description of articulated specimens

Cranial skeleton

In all CT-scanned specimens, the nasals and the frontals are separate, whereas the parietals are always fused. In all of the CT-scanned specimens (Fig. 3; Fig. 4; Fig. 5), in which the osteoderm cover was nearly completely removed from the skull by digital means, the dorsal surface of the skull-roofing bones is irregular, with some degree of sculpturing, primarily represented by grooves, on the anterior half of the parietal, on the frontals and on the nasals. Some tubercular-like structures are also visible, but these are probably artefacts of the CT-scan visualization, due to the incomplete removal of osteoderms. The suture between the frontals is bordered laterally by irregular and asymmetrical depressions.

In all specimens (Fig. 3; Fig. 4; Fig. 5), the skull is slender and elongate, with an average length to width ratio of 1.9. Its greatest width is across the quadrates. The premaxillae are separated at the midline by a deep vertical suture that is continued posteriorly by the internasal and interfrontal sutures. The narial openings are subtrapezoidal. Posteriorly, they are delimitated by the anterior

margins of the corresponding nasals; medially and anteromedially by the lateral margin of the nasal process of the premaxilla and by the maxillary process of the corresponding premaxilla, respectively; anterolaterally and laterally by the anterior border of the maxillae. The floor of each naris is formed medially and anteromedially by the expanded maxillary processes of the premaxilla, anterolaterally by the anterior processes of the maxilla and posteriorly by the septomaxilla. The nasals are trapezoidal, with subparallel margins that diverge slightly posteriorly to form posterolateral nasal processes, which contact the prefrontals laterally.

Together, the frontals start as slightly wider than the nasals, only to narrow in correspondence with the orbital constriction and then to widen again where they meet the anterior margin of the parietal. The posterior process of the prefrontal and the anteromedial process of the postfrontal almost entirely delimit the lateral borders of the frontals. Therefore, the frontals do not directly contribute to the orbital margin except for the small faceted expansions extending from the middle part of their lateral margins (Fig. 3: A; Fig. 4: A; Fig. 5: A). The posterior margin of the maxilla and the lacrimal contribute to the anteroventral border of the orbit, which is then continued dorsally by the prefrontal. The ventrolateral margin of the postfrontal thus constitutes much of the posterodorsal margin of the orbit, whereas only a small section of the anterior process of the postorbital bridges to the extremity of the posterodorsal process of the jugal, which connects the postorbital to the posterior process of the maxilla. Moreover, the triangular expansion of the palpebral bone interrupts the anterior margin of the orbit at the point where the maxilla and the prefrontal meet.

The parietal is longer than wide. Anteriorly it is almost as large as the combined posterior margins of the frontals, and then narrows slightly in the last third of the temporal fenestrae. Each temporal fenestra is an anteroposteriorly elongated rhomboid, defined anterolaterally by the medial margin of the postorbital, posterolaterally by the medial margin of the squamosal, anteriorly by the posterior margin of the postfrontal and medially by the lateral margin of the parietal (Fig. 3: A; Fig. 4: A; Fig. 5: A). In the articulated skull, the apical foramen of the quadrate is covered by the tip of the squamosal, which curves ventrolaterally to meet the cephalic condyle of the quadrate. The neurocranium is only partially covered by the parietal. In dorsal view, the posterior part of the neurocranium is convex, and its convexity is interrupted only medially by the opening of the foramen magnum (Fig. 3: A; Fig. 4: A; Fig. 5: A).

The palatal complex is clearly visible in ventral view (Fig. 3: B; Fig. 4: B; Fig. 5: B). The vomers appear to be fused, in contrast with the isolated bones of MDHC 427 (see below). However, this could also be due to an artefact of the CT-scan visualizations. The palatines, on the other hand, are completely separated at their midline, at the level of both the ventral and dorsal laminae. The pterygoids are as long as the vomers and the palatines together, connecting laterally to the

posterior part of the maxillae by the means of the sickle-shaped ectopterygoids. The palatal complex displays the following openings, anteroposteriorly ordered: the vomeronasal openings, the suborbital fenestrae, the interpterygoid vacuity. Each of the paired, trapezoidal vomeronasal openings are defined by the anteromedial margin of the palatal shelf of the maxilla and the anterolateral border of the vomer. The suborbital fenestrae are paired, almond-shaped openings: each fenestra is defined medially by the corresponding palatine, anterolaterally by the posterior palatal shelf of the maxilla, laterally and posterolaterally by the ectopterygoid and posteriorly by a tiny section of the anterior expansion of the pterygoid. The interpterygoid vacuity starts as the gap between the medial margins of the two palatines, widening posteriorly following the outward curvature of the pterygoids. This fenestra is closed posteriorly by the basisphenoid, the basipterygoid processes of which contact the pterygoids obliquely.

In lateral view (Fig. 3: C; Fig. 4: C; Fig. 5: C), the maxilla makes up most of the anterior part of the skull, and is continued posteriorly by the jugal bone, which, as mentioned before, constitutes the posterior margin of the orbit and rises obliquely to meet the postorbital bone. The posterior part of the skull is connected to the anterior part ventrally through the pterygoids, and dorsally through the skull-roofing bones and the postfrontal, postorbital and squamosal. The epipterygoids extend as slightly anteriorly-arched columns from the fossa columellae of each pterygoid to meet the ventral processes of the parietal and posteriorly to face the alar processes of the prootic. The quadrates are deeply arched around the stapes, contacting the sides of the neurocranium medially, the squamosal dorsally and the supratemporal posterodorsally.

No traces of an orbitosphenoid were found neither in the CT-scanned specimens nor in the disarticulated specimen.

Prior to the removal of the osteoderms, the ear opening was found to be very small compared to the size of the head (Fig. 6).

The mandibles bear a very tall coronoid matched with a dorsally elevated coronoid process of the dentary, which is clearly visible in lateral view (Fig. 3: F; Fig. 4: F; Fig. 5: F). In ventral view, the posterior part of the mandible, corresponding to the articular complex, is medially slanted. The articular complex contributes to almost half of the length of each mandible.

Postcranial skeleton

A complete rendering of the postcranial skeleton of *O. punctatissimus* was only available for CT-scanned specimen MCCI R776. In this specimen, the ratio of tail length to total body length is about 0.47 (Fig. 7). CT-scans of MCCI R775 and MCCI R952 included only the first nine or ten vertebral elements and the pectoral girdle. The morphology of the bones displayed in these scans was

comparable to that of specimen MCCI R776, albeit with some degree of variation in the pectoral girdle.

Vertebrae and ribs

In both MCCI R776 and in MDHC 427 the number of presacral vertebrae, including the atlas and axis, is 53. The two sacral vertebrae are therefore the 54^{th} and 55^{th} vertebrae of the column in both specimens. This count is not available for the other studied specimens. In MCCI R776, the two sacral vertebrae are followed by one anterior caudal vertebra and at least eight autotomic caudal vertebrae. The count of the posterior caudal vertebrae was hindered by the osteoderms in the CT-scan visualization. In the column, the first rib-bearing vertebral element is the fourth (Fig. 8) and ribs are borne by all subsequent presacral vertebrae. Dorsolaterally, the pectoral girdle inserts between the ribs of the third and the fourth postaxial vertebrae, with the scapulae not contacting the ribs laterally (Fig. 8). The cervical vertebrae, identified as those preceding the first vertebra with ribs contacting the sternum, according to the definition of Hoffstetter and Gasc (1969), are seven (Fig. 8). Each of these elements is also characterized by the presence of either a hypapophysis (in the anterior elements) or a distinct ventral keel (in the posterior elements). The transition from hypapophysis to keel is rather gradual.

The ribs are narrowly arched. In MCCI R776, a distal contact with two pairs of probably fully cartilaginous sternal ribs can be observed (Fig. 8).

Pectoral girdle

The pectoral girdle has the appearance of a ventrally convex kite (Fig. 9). The scapulae, which are not attached to the ribs, protrude from the lateral vertices of the girdle, contacting the clavicles with their anterior margin and being continued by the coracoids ventrally. In turn, the coracoids expand ventromedially, attaching to the sternum, which is probably cartilaginous and to which the sternal ribs are attached posteriorly. Anteriorly, the clavicles meet at the midline in MCCI R952 (Fig. 9: C), whereas they are separated by the anterior expansion of the interclavicle in MCCI R776 and MCCI R775 (Fig. 9: A, B, respectively).

The interclavicle is represented by a thin splint that seems to bear two symmetrical lateral expansions in MCCI R775, a more highly developed right one and an underdeveloped left one in MCCI R776, and none in MCCI R952. In all these specimens, it extends from where it meets the clavicles to the anteromedial margin of the sternum. Overall, some degree of internal asymmetry between the left and the right side of the girdle is evident in all specimens, especially in the

structure and attachment of the sternum, relative size of the coracoids and shape and positioning of the clavicles and the interclavicle. No vestigial elements of the forelimbs are present.

Pelvic girdle

The two single, symmetric elements of the pelvic girdle are inserted between the two sacral vertebrae. In MCCI R776, the two pelvic bones are positioned lateroventrally to the sacral vertebrae, gently arched and following the curvature of the inner body wall (Fig. 10). There is no connection between them and the vertebrae, and therefore, the pelvis is floating. No vestigial elements of the hindlimbs are present.

Description of isolated elements

Skull roof and suspensorium

Nasals

Nasals contact each other medially, the premaxilla anteriorly, the frontals posteriorly, the prefrontals posterolaterally and the maxillae laterally. The nasals are subrectangular, with an elongated anteromedial process protruding from the anteromedial corner (Fig. 11: A, B). This process contributes to almost one-third of the length of the nasal, terminating with a rounded distal end. Its dorsal surface is completely covered by the articulation surface with the nasal process of the premaxilla. The anterior margin and the medial margin of the nasal form an almost 90° angle, followed by a widening of the bone shelf posterolaterally, forming the enlarged posterior process, which has broad posterior contact with the frontal. In MDHC 427, the posterior half of the medial margin is pierced by three foramina, which are aligned in a parabolic fashion that moves away from the medial margin posteriorly. The posterior section of the lateral margin is somehow irregular, with a short, poorly defined laminar expansion, which is followed posteriorly by a small recess. No dermal ornamentation is present on the nasals.

Frontals

These are paired, rectangular bones (Fig. 12), overlapped by the nasals anteriorly, contacting the parietal posteriorly and the maxilla anterolaterally. They also contact the postfrontal posterolaterally and the prefrontal anterolaterally, which form part of the upper orbital margin. Since the posterolateral process is poorly developed, the frontals widen only slightly posteriorly, bearing poorly visible parietal facets for the articulation with the anterolateral processes of the parietal on the posterolateral side of the ventral surface (Fig. 12: C, D). The posterior margin is wider than the anterior one, and almost straight. The cristae cranii frontalis, two ventral descending flanges, each

extending from one third of the lateral margin of the frontals to the posterior end, extend ventrally to form anteromedially-directed and pointed processes interrupted by a small recess on their posteromedial side (Fig. 12: C, D, E). In dorsal view, the anterior margin of each frontal is strongly convex and terminates in a pointed medial process, whereas laterally it develops a small anteriorly-directed lateral process. A distinct nasal facet occupies most of the anterior margin, interrupted only by the anterolateral process and separated from the rest of the nasal shelf by a low ridge (Fig. 12: A, B). In dorsal and ventral views, the last third of the lateral margins of the frontals exhibit a distinct, rounded projection which is faceted anteriorly and posteriorly. The anterior surface is the posterior end of the prefrontal articular facet, whereas the posterior one is the anterior end of the postfrontal articular facet (Fig. 12: B). The frontals display some degree of dermal ornamentation in the form of grooves that are clearly visible on the dorsal surface of the bones.

Parietal

The parietal is a single, subrectangular bone constituting, together with the frontals, the main skull-roofing element of the skull. It contacts the frontals anteriorly, the postfrontals anterolaterally, the supraoccipital posteriorly, the otooccipitals, the supratemporals, and the squamosals posterolaterally, the epipterygoids ventrally.

In all specimens, the anterior edge of the parietal is straight except for a small indentation at the midline. Some dermal sculpturing is present on the dorsal surface of the parietal, but not strongly developed save for a slight thickening of the anterior margin. At the anterolateral corners of the parietal, the overlying parietal table curves backwards to reveal two clearly delineated and rounded anterolateral processes (Fig. 13: A). Those articulate with the parietal facets of the frontals.

The parietal foramen is located in the middle of the parietal table (Fig. 13: A; Fig. 13: B). In dorsal view, its margin is slightly raised and thickened to form a ring-like border. The posterior half of the lateral margin of the table displays two small flanges visible in dorsal and ventral view, which correspond to the points of origin of the two ventrally-directed epipterygoid processes (Fig. 13: C). These latter processes are clearly visible in lateral view.

The long and slender postparietal processes extending from the posterolateral edges of the parietal (Fig. 13: B) are slightly ventrally deflected, giving the parietal a dorsally arched appearance in lateral view (Fig. 13: C). These processes are distally rounded and contact the supratemporal and, in MCCI R775 and MCZ 38517, the squamosal laterally, whereas being in ventral contact with the dorsolateral surface of the neurocranium. Between these processes, and extending roughly half of their length, are two wedge-shaped posteromedial processes. Their subparallel medial margins define a deep and narrow parietal notch, which is shaped like a very narrow U in dorsal view (Fig.

13: A). The posterior section of the dorsal surface of the parietal, essentially comprising only the posteromedial processes and a small part of the posterior parietal plate shows two anteriorly rounded, anteroposteriorly slanted surfaces for the attachment of the temporal muscle (Fig. 13: A). The ventral surface of the parietal is smooth, except for the poorly-developed ventral crests. Of those, only the anterolateral and posterolateral crests touch each other (Fig. 13: B).

Premaxillae

Each of the paired premaxillae contacts the maxilla posterolaterally, the nasal posterodorsally, the vomer posteromedially and the other premaxilla medially. In all specimens, the external surface of the premaxillae shows no dermal ornamentation. In MDHC 427, the premaxillae partially coalesce near their base (corresponding to the alveolar border), but remain clearly unfused dorsally, with a nasal process divided lengthwise by a deep and narrow groove (Fig. 14: A, B). MCCI R775, MCCI R776 and MCCI R952 display a similar conformation. In lateral view, the ascending nasal process forms a 115° angle with the anterior shelf of the premaxilla (Fig. 14: C). At its base, the nasal process is wide, tapering towards its distal end, having an overall wedge-shaped appearance in anterior view. Moreover, due to the separation between the two halves of the nasal process, the septonasal crest is not clearly recognizable in posteroventral view. The vomerine processes of the premaxillae are well developed, with claw-like projections extending posteromedially and being clearly visible in lateral view (Fig. 14: C). The number of tooth positions in the dental shelf in specimen MDHC 427 is five, but only two evenly-spaced teeth, one in each half, are preserved. The same number of tooth positions was observed in MCCI R775, MCCI R776 and MCCI R952, but MCZ 38517 bears three tooth positions in each premaxilla. The tooth crowns are bicuspid, as in other scincids (e.g., *Scincella lateralis*; Townsend et al., 1999).

Maxillae

The maxillae contact the premaxilla and the septomaxilla anteriorly, the nasal dorsally, the palatine medially, the jugal posteriorly, the vomer and the ectopterygoid posteromedially, the frontal, the prefrontal and the lacrimal posterodorsally. They are roughly triangular, with a facial process tapering to form the dorsal apex of the triangle. The nasal facet, visible in lateral view (Fig. 15: B) on the dorsal tract of this process, is convex and separated from the posterior border of the narial opening by a small step.

In lateral view, on the posterior side of the maxilla, the facial process slightly overhangs the posterior process (Fig. 15: B). This long process (Fig. 15: B) constitutes the last section of the

maxilla, which in turn is rather straight for all of its length. It displays a convex ventral margin interrupted by a small step.

On the anterior part of each maxilla, two processes, an anteromedial and an anterolateral one, extend roughly parallel to each other in dorsal view, being separated by a deep notch (Fig. 15: E, F). The anteromedial process, which contacts the septomaxilla and the premaxilla, is dorsoventrally flat and characterized by a distinct dorsal lappet, which is slanted in the medial direction giving the process a forked appearance. The anterolateral process, which also contacts the premaxilla, is slightly longer than the anteromedial process and has a pointed tip.

In medial view, the palatal shelf of all specimens is straight (Fig. 15: D). The teeth appear to be bicuspid and have little to no difference in size. In MCCI R775, MCCI R776 and MCCI R952, the number of maxillary tooth positions is 12, whereas in MDHC 427 and MCZ 38517 each maxilla has ten and 11 tooth positions, respectively.

Jugals

The jugals are slender, L-shaped bones making up most of the posteroventral margin of the orbit. Each jugal comprises an anterior process and a posterodorsal process. The posterodorsal process is thin and elongated, retaining a constant width in lateral view and being twice as long as the anterior process (Fig. 16: A). A small jugal foramen is present at the contact between the anterior and posterodorsal processes (Fig. 16: A). The anterior process is slenderer and shorter than the posterodorsal process. At the meeting point of the two processes of the jugal, a small anteriorly-directed ventral step is present. No palatal or quadratojugal processes are present.

Lacrimals

The lacrimal is a small thin bone, resting along the ventral portion of the posterior margin of the facial process of each maxilla (Fig. 3: C; Fig. 4: C; Fig. 5: C). It is slender, being larger roughly at mid length and narrowing towards the anterior and posterior ends.

Prefrontals

The prefrontals (Fig. 17) are proportionally large bones constituting the anteromedial and anterodorsal margins of the orbit. The dorsal process is rather long and thin, with a slight expansion in the middle and a low palpebral crest being visible by its base on the lateral surface (Fig. 17: A). This process contacts the cristae cranii of the frontal. The anterodorsal process (Fig. 17: A) is convex and widely rounded. A wide notch for the lacrimal foramen separates it from the narrower

posteroventral process, which is squared. A squared orbitonasal flange projection is present ventrally to the dorsal process (Fig. 17: B).

Postfrontals and postorbitals

The postfrontal (Fig. 18: A, B, C, D) is a Y-shaped bone that contacts the frontal, the parietal, the jugal and the postorbital. In dorsal view, it displays a long and rounded anteromedial process and a shorter and more rounded lateral process (Fig. 18: A, B, C, D). These processes are connected by a concave anterior margin. The anteromedial process is long, with a smoothly curved posteromedial margin. More posteriorly, the postfrontal tapers in correspondence with the frontoparietal contact. Posteromedially, the thin shaft of the postfrontal widens and displays a small concavity that leads to the pointed posterior projection. The margin thus defined constitutes the anterior margin of the temporal fossa. Both, the dorsal and ventral surfaces of the postfrontal are smooth.

The postorbital (Fig. 18: E, F) is a rod-shaped bone that connects the posterolateral margin of the postfrontal to the anterior tip of the squamosal. It is curved anteroventrally and slender in dorsal view, having broad contact with the medial margin of the squamosal. It comprises a short anterolateral process and a long posterior process, the distal ends of which are both pointed.

Squamosals

The squamosal (Fig. 18: G, H) is an elongated bone that forms the dorsolateral margin of the skull. Its shape, as described by Evans (2008), is similar to that of a "hockey stick", with a straight and elongated main body hooking posteriorly to contact the cephalic condyle of the quadrate from a dorsomedial angle. The medial portion of this hook contacts the postparietal process of the parietal. In MDHC 427, the curvature of the squamosal is gentler, whereas it is more abrupt in MCCI R775, MCCI R776 and MCCI R952. At least in the articulated specimens MCCI 775 and MCZ 38517, the squamosal has a small contact with the postparietal process of the parietal near the apex of the curvature. The anterior process of the squamosal is straight and tapers anteriorly to a point. It contacts the postorbital anteromedially.

Quadrates

The quadrates (Fig. 19) are D-shaped in lateral and medial view. They contact the otooccipital dorsomedially, the supratemporal dorsally, the squamosal dorsolaterally, the pterygoid ventromedially and the articular ventrally. The dorsal end of the quadrate, the cephalic condyle, is strongly expanded posteroventrally. It is connected to the ventral end, the mandibular condyle, by a columnar body from which an arched lateral lamina originates (Fig. 19: A). The lateral lamina is not

much expanded laterally and is characterized by a convex swelling in its dorsal portion. In anterior view, the columnar body expands slightly ventrally (Fig. 19: B, C) starting at the top of the cephalic condyle. There are no evident foramina near the cephalic and mandibular condyles. The mandibular condyle is divided into two rounded articular surfaces separated ventrally by the condylar notch. The medial lamina, which starts at the cephalic condyle and is poorly developed, takes its origin medial to the central column.

Supratemporals

The supratemporals (Fig. 20) are curved bones contacting the posterolateral surface of the neurocranium. They insert between the medio-dorsal margin of the posterior turn of the squamosal and the lateral margin of the postparietal processes of the parietal. Each supratemporal is larger in the middle and tapers towards the ends.

Palpebrals

The palpebrals (Fig. 21) are recognizable only in the CT-scanned specimens (MCCI R775, MCCI R776 and MCCI R952). They are small, flattened and triangular bones that loosely contact the prefrontal. There is a slight convexity on the medial margin of each palpebral where it contacts the prefrontal. The posterior margin is concave.

Palatal complex

Septomaxillae

The septomaxillae (Fig. 22) are small bones positioned between the premaxilla, maxilla and vomer, lying on the floor of the external naris. They cover the vomeronasal apparatus dorsally. In ventral view, the concavity for the vomeronasal apparatus, the concha vomeronasalis, is clearly visible. Dorsally, the surface of each septomaxilla forms the anteroventral part of the nasal capsule. A subtriangular posterolateral process develops from the septomaxilla posterolaterally (Fig. 22: A). This process contacts the anterior part of the maxilla medially. A second, narrower anterolateral process (Fig. 22) develops anterolaterally, extending into the cavity of the external naris.

Vomer

The vomer (Fig. 23) is a bone constituting the anterior part of the palatal complex. In the CT-scanned specimens MCCI R775, MCCI R776 and MCCI R952, it appears as a single element comprised of two fused halves (possibly resulting from an artefact in the CT-scan visualization), whereas in MDHC 427, the paired vomers are not fused. Anteriorly, each half of the vomer displays

an anteromedial process that contacts the palatal processes of the premaxillae. In all specimens, this process is pierced by a small vomerine foramen. Posterolaterally, the anteromedial process narrows to a round concavity, which constitutes the medial margin of the vomeronasal opening. Posterior to this, the vomer develops into a laterally-expanded lamina, which makes a broad contact with the palatal shelf of the maxilla. The lateral lamina retains roughly the same width for two thirds of the vomer and then tapers to a pointed posterolateral process that is separated from the posteromedial process of the central lamina by a V-shaped notch.

Palatines

The palatines (Fig. 24) are bones that constitute the middle element of the palatal complex. Each palatine is subdivided into a ventral and a dorsal lamina enveloping the choanal duct. The dorsal lamina runs parallel to the dorsal lamina of the other palatine for more than half of its length, never contacting it. The ventral laminae extend halfway through the mediolateral distance covered by the dorsal laminae, again without midline contact. Anteromedially, the dorsal lamina folds into a ventral expansion that tapers to a point in the vomerine process, through which the palatine contacts the vomer. This process is much shorter than the triangular anterolateral projection of the ventral lamina (Fig. 24: A, B, C, D). Anterolaterally, the palatine develops into a small and trapezoidal maxillary process, which has an articulation surface with the maxilla ventrally. It also extends up to the anterolateral projection of the ventral lamina. A complete infraorbital foramen develops on the dorsolateral surface of this process, near the point where it converges into the dorsal lamina.
Posterodorsally, the palatine displays a pterygoid process, which expands laterally to broadly contact the anterior shelf of the pterygoid (Fig. 24: B, C). In all specimens, both the dorsal and the ventral surfaces of the palatines are smooth and there are no palatine teeth on the ventral surface.

Pterygoids

The pterygoids (Fig. 25) are the posteriormost elements of the palatal complex. These Y-shaped, bones are comprised of the elongated and posteriorly-directed quadrate process, the anteromedially-directed palatine process and the anterolaterally-directed pterygoid flange. The palatine process (Fig. 25: A, B) is very short and thin in lateral view, terminating in a widely rounded tip. This process is connected to the pterygoid flange by a thin shelf with a wavy anterior margin, on which a small U-shaped pterygoid recess is visible. The pterygoid flange is delineated by the underlying ventral ridge that is clearly visible in ventral view (Fig. 25: C, D). In ventral view, the pterygoid shelf exhibits one foramen anterior to the ventral ridge, as well as a clearly distinguishable ectopterygoid facet. A second ectopterygoid facet is also clearly delineated in dorsal view by the

presence of a well-developed dorsal ridge along the dorsal surface of the pterygoid flange. In ventral view, the pterygoid teeth are absent in all specimens except MDHC 427 and MCZ 38517. Both of the latter two specimens have three teeth on the right element, whereas one tooth is visible on the left element of MDHC 427 and two are present on the left pterygoid of MCZ 38517. However, considering empty tooth positions the number of teeth in the left pterygoids is probably three as well. The pterygoid teeth appear to be quite enlarged in relation to the size of the pterygoid (Fig. 25: C, D, E, F). The quadrate process (Fig. 25: B, C) of the pterygoid is long and terminates into a rounded tip corresponding to the articulation with the quadrate. In dorsal view, the fossa columellae is located at the proximal end of the quadrate process to accommodate the epipterygoid. The fossa appears to be closed posteriorly and is either circular or elliptical.

Ectopterygoids

The ectopterygoids (Fig. 26) are small sickle-shaped bones. Each ectopterygoid connects the jugal and the maxilla to the pterygoid. It comprises the maxillary process, a curved and pointed structure that contacts the jugal and the maxilla anteriorly, and the ventral and anteromedial lappets, two thin, similar-sized and parallel processes grasping the pterygoid flange of the pterygoid, both ventrally and dorsally (Fig. 26: A, B).

Epipterygoids

The epipterygoids (Fig. 27) are columnar bones connecting the pterygoid with the contact between the descending process of the parietal and the alar process of the prootic. The base of each epipterygoid is slightly enlarged. The epipterygoid is somewhat anteriorly curved through its length, forming a gentle arch.

Neurocranium

Stapes

The stapes (Fig. 28) is a small, elongated bone of the auditory system that does not directly articulate with any other neurocranial bone. It is a thin rod, enlarged only at its medial end. The footplate of the stapes, inserted in correspondence with the foramen ovale, is larger than the lateral end, which extends posteriorly to the quadrate to the external meatus. This bone does not exhibit a stapedial foramen.

Supraoccipital

The supraoccipital (Fig. 29: A) is an unpaired, gently arched element forming the posterodorsal roof of the braincase. In all studied specimens, it displays a strong degree of fusion with the otooccipitals and the prootics, therefore, its shape is hardly distinguishable as subhexagonal and convex in dorsal view. Its dorsal surface is smooth, bearing only small traces of the emerging semicircular canals. The posterior margin of the supraoccipital is concave and smoothly shaped as an inverted U and forms the dorsal margin of the foramen magnum. From the anterior part of the bone, a short processus ascendens (Fig. 29: A, D, E) extends, which fits into the corresponding posteromedial fossa of the parietal. This small, dorsoventrally compressed process terminates with a truncated end. The anterior end of the contact with the prootics is marked by small marginal processes.

Prootics

The prootics (Fig. 29: A, C, D) are bones constituting the anterolateral part of the neurocranium. Each prootic comprises an alar process (Fig. 29: A, C) and an anterior inferior process (Fig. 29: C), converging to a common base, which in turn extends posteriorly into the main body of the prootic, the posterior process, from which the paroccipital projection originates posteriorly. The alar process is a long, anteriorly directed and almost vertical, subtriangular expansion, the anterior edge of which shows a slight medial inflection. Ventrally, the anterior inferior process constitutes the posteroventral margin of the incisura prootica, which separates this process from the alar one (Fig. 29: C). The anterior inferior process is lateroventrally bordered by the crista prootica. This crest is very low and continues posteriorly into the posterior process. The paroccipital projection extends posteriorly from this latter process. The projection is an almost indistinguishable posterior expansion similar to a truncated triangle that meets the anterolateral part of the otooccipital in correspondence with the otic capsule. The anterior end of the contact between the supraoccipital and the prootics is marked by a small marginal process.

Otooccipitals

The otooccipitals (Fig. 29) are bones making up most of the posterolateral portion of the neurocranium and the lateral margins of the foramen magnum. They are also the neurocranial bones that are pierced by the greatest number of foramina. Each is constituted by the complete fusion of the exooccipital and the opisthotic. Posteroventrally, the otooccipital expansions form the two smoothly rounded lateral thirds of the occipital condyle, the third, central part being the contribution of the basioccipital (Fig. 29: E). Dorsal to the condyle, the posterior margin of the otooccipital develops into a gentle concavity, forming the lateral margins of the foramen magnum. Near the ventrolateral edge of the foramen magnum, two foramina for the vagus nerve and the hypoglossal

nerve open (Fig. 29: E). Some specimens seem to show a higher number of hypoglossal foramina (e.g., three or more in MCCI R952). A distinct crest, the crista tuberalis, develops anterolaterally to these foramina (Fig. 29: C). In lateral view, this crest is obliquely-directed, starting from the ventrolateral edge of the foramen magnum and terminating anteroventrally to contact the enlarged sphenooccipital tubercle of the basioccipital, thus constituting the posterior edge of the lateral opening of the recessus scalae tympani. The recessus is a small, almost vertical and elliptical concavity, located on the ventrolateral part of the otooccipital. Anterior and subparallel to the crista tuberalis, the crista interfenestralis, a small fold of bone developing posteriorly to the foramen ovale, contributes to the anterior enclosure of the recessus scalae tympani (Fig. 29: C).

A third crest develops dorsolaterally to the position of the vagus and hypoglossal foramina, forming the posterior border of the paroccipital process. This process is very short and projects dorsolaterally, forming an almost vertical, thick expansion. The anteroventral surface of the paroccipital process articulates laterally with the cephalic condyle of the quadrate and dorsolaterally with the supratemporal.

Basioccipital

Of the two unpaired bones that constitute the basicranium, the basioccipital is the posterior one (Fig. 29: B). It is the largest of the two elements, making up more than two-thirds of the basicranial complex. It is ventrally convex and roughly hexagonal and culminates posteriorly with the constriction associated with the occipital condyle. It contacts the sphenoid anteriorly, the prootics anterolaterally and the otooccipitals posterolaterally. The two lateral vertices of the hexagon form the sphenooccipital tubercles (Fig. 29: B).

Sphenoid

The sphenoid (Fig. 29: A, B, C, D) is a moderately short element constituting the anterior part of the basicranium. It forms by the fusion of the basisphenoid and parasphenoid. It presents two short, axe-shaped and well-developed basipterygoid processes. These processes are distally expanded and contact the pterygoids with their dorsal convex articular surfaces. In anterior view, the anterior openings of the Vidian canals are clearly visible right next to the expansions of the basipterygoid processes.

In MDHC 427 and MCZ 38517, on both the dorsal and the ventral surfaces of the sphenoid, the horizontal line of the suture with the basioccipital shows a slight medial indentation. More anteriorly, the crista sellaris rises roughly parallel to the suture line, separating the sphenoid into an anterior and a posterior section, and marking the posterior margin of the sella turcica. No

parasphenoid rostrum is present, whereas the trabeculae cranii are very poorly developed. The anterior section of the sphenoid is characterized by the sella turcica, a deep and subtriangular central concavity, which is defined laterally by two crests that converge to the anterior point of the sphenoid and posteriorly by the crista sellaris. Dorsally, the sella turcica is covered by a short dorsum sellae. Vertical and laminar supravenous processes are visible by the bases of the basipterygoid processes. These processes merge with the crista prootica posteriorly. Each posterolateral corner of the sphenoid bears a short crista ventrolateralis.

Inner ear (bony labyrinth)

The hollow bone structures of the inner ear, also called the bony labyrinth, are completely enclosed within the dorsolateral parts of the neurocranium (the prootics and the otooccipitals). They are not visible externally except for the dorsal culminations of the semicircular canals. In lateral view (Fig. 30; Fig. 31; MCCI R776 not figured), the foramen ovale represents the only opening of this complex system of cavities. In the complete skull, the stapes is inserted perpendicularly to this foramen. *Ophiomorus punctatissimus* displays a moderately large and relatively rounded vestibule in its inner ear, enclosed within the space defined anteriorly by the anterior semicircular canal and posteriorly by the posterior semicircular canal. In lateral view, the lateral semicircular canal constricts the vestibule on the horizontal plane. Each of these canals is characterized by a tubular appearance, retaining a constant diameter for all its length and then enlarging to form an ampulla. The ampullae of the anterior and lateral semicircular canals are positioned respectively on the anterior and anterolateral sides of the vestibule, contacting each other, whereas the posterior semicircular canal forms an ampulla on the posterior side of the vestibule.

Lower jaw

Articular complex (compound bone)

The articular, the prearticular and the surangular are fused into these composite and mediolaterally compressed elements (Fig. 32). The complex is comprised of the retroarticular process, the articular condyle and the prearticular spine. The retroarticular process (Fig. 32: B) is a somewhat concave, rectangle-shaped process with rounded edges. It makes up about 20% of the length of the complex and is located posteriorly and ventrally inflected at an obtuse angle to the rest of the articular complex. In medial view, this process displays a thick tympanic ridge running almost along its entire length, which is dorsoventrally expanded at the posterior end of the process (Fig. 32: D).

The articular condyle is roughly square-shaped and posterodorsally directed, with two small facets for the insertion of the mandibular condyle of the quadrate. Anterior to the condyle is a medially-directed protuberance that tapers to a pointed tip.

The prearticular spine (Fig. 32: C) is composed by the surangular and the prearticular. It has a relatively narrow and anteroposteriorly elongated form, terminating in two pointed processes (the upper one is part of the surangular, whereas the lower one is part of the prearticular) roughly equal in length. This component of the complex contacts the dentary. In medial view, the two processes are separated, showing the incomplete fusion between the surangular and the prearticular. At the posterior end of the prearticular spine, anterior to the articular condyle, the adductor fossa opens for the insertion of the adductor muscle. This fossa is narrow and elongated. In MDHC 427, MCCI 775 and MCCI 952, it tapers to an anterior point (Fig. 32: C, D; Fig. 4: G; Fig. 5: G), whereas in specimens MCCI 776 (Fig. 3: G) and MCZ 38517 it is more rounded.

In lateral view (Fig. 32: A, B), the articular complex is smooth. In the anterodorsal part of the bone, a small and elongated anterior surangular foramen is present, whereas the more rounded posterior surangular foramen pierces the posterodorsal part of the bone just anterior to the articular condyle. The anterodorsal part of the bone also displays a clearly visible depression for the contact with the dentary, the dentary facet, whereas ventrally it displays an articular surface for the angular.

Coronoids

The coronoids (Fig. 33) are bones that form the dorsalmost element of the mandible, articulating medially with the surangular and the prearticular, anteriorly with the dentary and anteromedially with the splenial. They are crescent-shaped bones with a dorsal extension (the coronoid process) giving them an appearance similar to an inverted V. Only in MDHC 427, the whole structure of the coronoid is clearly visible due to its disarticulated state.

Protruding from the anterior part of the coronoid, the anteromedial process is a spur of bone with a thin, relatively elongated sheet descending from it (Fig. 33: A, C). Posteriorly, this sheet displays a very small step on the backside of the anteromedial process. Longitudinally, the medial side of the anteromedial process is divided into a dentary facet (dorsally) and a splenial facet (ventrally). The lateral side displays only a shallow dentary facet (Fig. 33: B). The coronoid ridge is a strong and relatively well-developed crest descending medially from the coronoid process to the posteromedial process.

In lateral view, the labial process is widely rounded, anterolaterally directed and very poorly developed (Fig. 33: A, B). Posteriorly, the coronoid develops into a rounded posteromedial process (Fig. 33: C, D), slightly elongated in posteroventral direction. Dorsally, this process slightly

expands into a very poorly developed posterior process, which is almost absent in some specimens (e.g., MDHC 427).

Splenials

The splenial (Fig. 34) is a laterally compressed splint of bone, which contacts the dentary, the coronoid and the articular complex. It covers the medial side of the lower jaw in its anterior portion, starting below the coronoid with a pointed tip. It then expands anteriorly towards the dentary, where it bifurcates to form a deep, wide anterior concavity, the anterior inferior foramen (Fig. 34: A). Posteroventrally is a small notch for the insertion of the angular, whereas a small, rounded anterior mylohyoid foramen is present in the middle of the bone (Fig. 34: A). The dorsal crest, running dorsally to the concavity of the anterior inferior foramen, is not very pronounced.

Dentaries

The dentaries are the longest and only tooth-bearing elements of the lower jaw (Fig. 35). Each dentary contacts the coronoid, the surangular and the prearticular posteriorly, the splenial medially and the other dentary anteromedially in correspondence with the mandibular symphysis, which in all specimens is narrow and almost horizontal. In MDHC 427, both, the right and the left dentaries have a total of 13 tooth positions, whereas in MCZ 38517, they have 14, and in MCCI R775, MCCI R776 and MCCI R952, the number of dentary tooth positions is 15. The teeth are pleurodont and appear to be bicuspid, with smaller teeth anteriorly which generally increase in robustness towards the posterior end of the tooth row. In medial view, a thick subdental shelf (sensu Rage & Augé, 2010) develops underneath the teeth, with its ventral part constricting the Meckelian fossa, but leaving it open for all its length (Fig. 35: C, D). A distinct subdental ridge is present dorsally on the shelf. The coronoid facet on the posterior part of the shelf is individuated by an obtuse angle.

On their lateral surfaces, the dentaries display a varying number of small foramina (Fig. 35: A, B), of which the anteriormost is located almost ventrally near the anterior end of the bone. Up to five foramina are present in MDHC 427 and MCCI 952, whereas MCZ 38517, MCCI R775 and MCCI R776 show up to six of them. The number of foramina can be different in the two dentaries of the same specimen (e.g., MDHC 427 has four foramina in the left dentary and five in the right dentary; Fig. 35: A, B).

The posterior end of the dentaries develops into three distinct posterior processes: the dorsal (coronoid) process, the central (surangular) process and the ventral (angular) process (Fig. 35: C, D). The dorsal posterior process is dorsoventrally thick and mediolaterally thin, with a slightly concave dorsal margin and a slightly rounded tip. Being strongly dorsally deflected, this process

forms an angle of roughly 135° with the dorsal margin of the dental shelf. The central posterior process is located between the other two and is posteriorly directed, terminating in a tip somewhat thinner and sharper than that of the coronoid process. The dorsal margin of this process is straight and forms an acute angle with the ventral margin of the dorsal process. The ventral posterior process is posteriorly directed, terminating with an irregularly rounded tip.

Angulars

The angular bone (Fig. 36) is small and elongated. It contacts the ventral part of the articular complex dorsomedially, the dentary anterolaterally and the splenial anteromedially. Anteriorly, it develops a thin process that is entirely overlapped by the dentary and the splenial in the articulated skeleton.

Hyoid apparatus

The hyoid apparatus (Fig. 37) is positioned ventrally to the neurocranium, but it has no direct contact with it. It is comprised of an anterodorsally oriented, unpaired stick-like element identified as the basihyal anteriorly, which is fused to the processus lingualis. The basihyal is followed posteriorly by two arched elements, the first ceratobranchials.

Axial skeleton

Atlas

The atlas (Fig. 38) is the first element of the vertebral column, articulating with the occipital condyle anteriorly and with the axis posteriorly. It is composed of three unfused elements, the intercentrum and the two portions of the atlantal neural arch. As seen in the CT-scans, the intercentrum is positioned ventrally between the other two elements. It is a small, triangular bone. The ventral vertex of which is represented by a short and thick keel (Fig. 38: B). The separated portions of the neural arch are C-shaped in anterior and posterior view, with a 90° angle between the dorsal extension of the arch and its ventral ramus. The dorsal extension of the arch is dorsoventrally flat and obliquely oriented in anterior view. On its posterior margin, it displays a small, triangular projection matching a corresponding anterior cavity in the axis. The ventral ramus (Fig. 38: A, B) is expanded to form a medioventrally-oriented, concave articular surface posteriorly, which clasps the odontoid process of the axis from a dorsolateral angle in the articulated specimens.

Axis

The axis (Fig. 39) is the second cervical vertebra, articulating with the atlas anteriorly and with the third cervical vertebra posteriorly. It is a relatively large element if compared with the atlas, bearing a completely-fused neural arch topped by a neural spine. The axis is completely fused to the odontoid process, thus having a biconvex centrum (Fig. 39: C). The anterior articular surface of the axis is rounded, and wider than high, with the odontoid process protruding from it mediodorsally. The ventral surface of this process is concave, whereas its dorsal surface is slightly convex in correspondence with the anteroventral edge of the axial neural canal. The anterior articular condyle also displays a complex and well-developed ventral keel: following a short vertical step, this laterally-compressed, longitudinal keel descends posteroventrally. Its distal end bears a small dorsal expansion. The posterior margin of the keel is deeply concave, and in MDHC 427, it displays a small posteriorly-directed bony spur just ventrally to the attachment to the centrum. After a small concave tract, which is marked by a short ventrally-directed spur in MDHC 427, this anterior keel is followed by a second ventral keel on the posterior intercentrum of the vertebra. This second keel is longer than the first one and forms a 60° angle with the posterior intercentrum. Its distal end is slightly enlarged anteroposteriorly, bearing a small, anteriorly-directed triangular spur on its anterior margin and a larger, rounded expansion with a small dorsal concavity on its posterior margin. The posterior condyle for the articulation with the third cervical vertebra is almost hemispherical, being only slightly dorsoventrally depressed in posterior view (Fig. 39: E). Lateral to the main body of the anterior intercentrum, the vertebral lamina expands on both sides of the vertebra to form two flat, obliquely-oriented processes.

The neural arch of the axis encloses the neural canal together with the neural canal floor. The basal part of each side of the arch, the neural pedicel, has a concave anterior margin and a convex posterior margin. Dorsal to the posterior margin, the spinopostzygapophyseal lamina (SPOL) runs dorsally from the postzygapophyses. Starting from each postzygapophysis, the SPOL becomes concave before contacting the neural spine (Fig. 39: D, E). The postzygapophyses bear small posteroventrally-slanted articular surfaces for the prezygapophyses of the following vertebra. The anterior lamina is also concave. The dorsal margin of the neural spine is almost horizontal if compared to the neural canal floor, and, in the CT-scanned specimens, it is laterally expanded at the distal end. In posterior view, the neural arch is wide (Fig. 39: E).

Postaxial cervical vertebrae

The anterior postaxial cervical vertebrae (Fig. 40: A, B, C, D, E) are characterized by prominent hypapophyses extending from the middle of the ventral surface of the centrum. Descending in ventral direction, a hypapophysis has an expanded proximal half and then tapers to a distinct

laminar structure. In dorsal view, the anterior postaxial cervical vertebrae display an anterodorsally elongated neural spine (Fig. 40: A). By the sides of the spine, the postzygapophyses are quite short, whereas anteriorly the vertebra bears two distinct and oval prezygapophyses. Lateral to the main body of the vertebra, the vertebral lamina expands on both sides to form two anterodorsally-flattened, obliquely-oriented processes. On the anterior surface of the distal end of these processes, a small concavity is present (Fig. 40: D).

The posteriormost cervical elements (Fig. 40: F shows the last cervical element, that is the seventh vertebra, in posterior view) are different from those located anteriorly. The main difference is the lack of a distinct hypapophysis. Instead, they display a short ventral keel. The lateral processes are also replaced by thick synapophyses.

Trunk vertebrae

The trunk vertebrae do not show a significant degree of variation throughout the vertebral column. All trunk vertebrae have procoelous centra, with a rounded, dorsoventrally-compressed posterior condyle contributing to one-third of the length of the centrum in lateral view (Fig. 41: A, B). The anterior cotyle is also rounded and dorsoventrally-compressed in anterior view, and narrower than the neural canal. The vertebral centrum of the trunk vertebrae is slightly more elongated than that of the cervical vertebrae. The pedicels are longer than they are high. Their anterior margin is concave. Anteriorly, a thickened, almost vertical synapophysis is present on each side of the neural arch. In lateral view, the neural spine forms a 30° angle with the neural canal floor (Fig. 41: C). In some of the vertebrae, in proximity to the posterior condyle, the neural canal floor shows a small, dorsally flat bridge bordered by two shallow depressions (Fig. 41: E). Some of the largest vertebrae also show one or two large foramina on the anterior third of the ventral surface of the centrum. These foramina are absent in the smallest vertebrae. When two foramina are present in a single vertebra, they generally differ in size from one another. In the vertebra figured in Fig. 41, for example, the left foramen is smaller and subcircular, whereas the right foramen is larger and more elongated (Fig. 41). A low keel runs through the length of the centrum, separating the foramina when two of them are present. In all trunk vertebrae, the prezygapophyseal facets are dorsoventrally slanted at 45° and anterolaterally directed, with an oval shape in dorsal view. The postzygapophyses are also oval in ventral view and similarly inclined.

Sacral vertebrae

The two sacral vertebrae (Fig. 42) are distinguishable from the presacral ones by the presence of the transverse processes and by the slightly less dorsoventrally compressed centrum. In the rest of their

morphology, they are practically identical to the trunk vertebrae. These two vertebral elements are not fused in any of the examined specimens. The first sacral vertebra has slightly shorter, anteriorly arched transverse processes (Fig. 42: A, B, C). The distal ends of these point posteriorly. The second sacral vertebra has longer and straighter transverse processes, which slightly enlarge at their distal ends to form a lateroventrally-facing flat surface (Fig. 42: F, G, H). In MDHC 427, the transverse processes of the first sacral vertebra are shorter and subhorizontal in anterior view, whereas in MCCI R776 they have roughly the same orientation as the transverse processes of the second vertebra. Furthermore, in MDHC 427, the distal ends of the transverse processes of both vertebrae are slightly asymmetrical, with the right transverse processes being slightly longer and, in the case of the second sacral vertebra, with a more ventrally-slanted distal end. A similar asymmetric condition is also shared to a minor degree with the CT-scanned specimen MCCI R776. In MCCI R776, the transverse processes of the first sacral vertebra do not contact those of the second sacral vertebra.

Non-autotomic caudal vertebrae

Each of the examined specimens has a single non-autotomic caudal vertebra (Fig. 43) that follows the sacral vertebrae and precedes the autotomic caudal ones. Its morphology does not differ significantly from that of the sacral vertebrae, except for the slightly shorter transverse processes and the body of the vertebra being shorter. At their distal ends, the transverse processes are bifid. The centrum, and consequently the anterior cotyle and the posterior condyle, are more dorsoventrally flattened than those of the sacral vertebrae, approaching the presacral condition.

Autotomic caudal vertebrae

The posterior caudal vertebrae are thinner and more elongated than the other vertebrae. They display the autotomy plane that separates the vertebra into two portions (Fig. 44: A, B). The autotomy plane is marked by a raised suture, which displays an anterior convexity on the dorsal surface of the vertebra. The anterior portion of the vertebra bears a slightly concave, almost flat anterior cotyle, whereas the posterior condyle on the posterior portion is round and posteriorly expanded in ventral view. The posterior condyle is also smaller in diameter than the main body of the vertebral centrum. In posterior view, the ventral margin of the centrum is characterized by two rounded lateral concavities interrupted ventromedially by a round notch. These are the articulation surfaces for the chevron bone. The neural spine, present only on the posterior portion of the vertebra, develops posterodorsally. In dorsal view, the postzygapophyses are rounded, reaching further posteriorly than the neural spine. Anteriorly, the posterior element develops into two

anterolaterally-directed transverse processes, which are pointed on their distal ends. The anterior element contributes to two-thirds of the anterior margin of these processes by forming two small pointed processes. Between the anterior and posterior transverse processes, a small gap or indentation is recognizable in ventral view, representing the continuation of the vertebral fracture plane between the transverse processes. This means that the autotomic vertebrae of *O. punctatissimus* can be identified as belonging to the "converging process" type, as defined by Etheridge (1967).

Ribs

The ribs (Fig. 45) are elongated and curved elements articulating with the synapophyses of the dorsal vertebrae. The head of the rib is enlarged and hosts a squared, shallow depression.

Appendicular skeleton

Clavicles

The clavicles (Fig. 46: A, B, but see also Fig. 9) are S-shaped and slender bones contacting each other at the anteromedial end of the pectoral girdle and posterolaterally the coracoid and scapula. The medial point of contact between the two clavicles develops into a posteriorly-directed expansion to which the interclavicle articulates. Regarding the shape and structure of the clavicles, a significant degree of variation exists between the studied specimens. The anterior arch of the clavicles appears to be relatively wider in MCCI R776, MCCI R775 and MDHC 427 than it is in MCCI R952. The posterior turn of the clavicles of MCCI R952 bears a small posteriorly-directed expansion, which is absent in all remaining specimens. While absent in all other specimens, the traces of an open perforation of the clavicle are evident in MCCI R775, especially in the left element, where a medially directed spur originates from the posterior margin of the bone, whereas in the right element the spur is smaller and more posteriorly directed (Fig. 9: B).

Scapulae

The scapulae (Fig. 46: C, D, but see also Fig. 9) are bones constituting the dorsolateral part of the pectoral girdle. In all CT-scanned specimens of *O. punctatissimus*, they are small, flattened elements located between the second and the third cervical ribs, to which they are not connected directly. The dorsal end of the scapulae is somewhat expanded to form a thin sheet of bone, the margins of which appear to be partially unossified and probably cartilaginous. The rest of the scapula is represented by an elongated and slender process, which contacts the coracoid bone distally and the clavicle on its anterior margin. The margin of the dorsal expansion of the single

scapula available in MDHC 427 is well defined, albeit it is a bit less expanded than that of MCCI R775, MCCI R776 and MCCI R952.

Interclavicle

The interclavicle (Fig. 9) appears as a short and slender stick that can bear two more or less symmetrical lateral expansions (Fig. 9: A, B) in some specimens (MCCI R775 and MCCI R776). It connects the posterior part of the medial expansions of the clavicles to the anterior margin of the sternum. It was not found in MDHC 427, but it is clearly visible in all CT-scanned specimens.

Coracoids

The coracoids (Fig. 46: E, F, but see also Fig. 9) are elongated bones contacting laterally the ventral process of the scapula and the posterior margin of the lateral part of the clavicle with a rod-like lateral portion. Ventromedially, each coracoid expands into a flat, axe-shaped sheet, which is the point of attachment for the anterolateral expansions of the sternum. In MDHC 427, the ventral sheet of the coracoid is much larger than the dorsal sheet of the scapula.

Sternum

This element can be only seen in the CT-scans (Fig. 8; Fig. 9). The presternum is clearly recognizable in all scanned specimens. It is probably unossified, appearing as a thin, backward-pointing, subtriangular sheet that is symmetrically attached to the enlarged medial expansions of the coracoids. It contacts the posterior end of the interclavicle anteromedially. The presternum is rather short, being distinctly wider than long. Its flat ventral surface appears to be in broad contact with the ventromedial section of the body wall. A small expansion is visible in the middle of the posterior margin of the presternum in MCCI R776 and maybe also in MCCI R952. This expansion might represent the mesosternum. It is not visible in MCCI R775, but this could be due to a matter of resolution of the scan. Two sternal ribs contact the posterolateral margins of the sternum on each side. The first pair of ribs meet the posterolateral margins of the presternum in the middle, whereas the second pair contact the supposed mesosternum.

Pelvic girdle

All examined specimens of *O. punctatissimus* bear vestigial pelvic elements, which can be recognized as an almost completely undifferentiated fusion of ilium, ischium and pubis (Fig. 47). The ilium is the most recognizable. It is represented by an elongated and laterally arched dorsal process, expanding into a more enlarged main body ventrally. The ventral part of the girdle bears a

downward-facing pointed process not much differentiated from the rest of the girdle, which can be interpreted as a puboischium.

DISCUSSION

Asynchronous loss of limbs in *O. punctatissimus*

Limb loss and reduction evolved at least 16 to 20 times independently across Scincidae, corresponding to a very high frequency of convergent limb loss among squamates (Wiens et al., 2006; Siler and Brown, 2011; Miralles et al., 2012, 2015). Within Scincidae, the genus *Ophiomorus* exhibits a highly interspecifically variable degree of limb reduction, but the reduction of digits, if present, is stronger in the hindlimbs than in the forelimbs (Greer and Wilson, 2001).

The extremely regressed status of the appendicular skeleton of *O. punctatissimus* gives clues about the evolution of limb loss in this species. A previous study based on radiographs by Andrade et al. (2016) regarding the appendicular skeletons of five skinks included also *O. punctatissimus* and argued that the pectoral girdle of this species was only comprised of a mostly cartilaginous scapula, an interclavicle and a clavicle. The material studied herein provided a slightly different account: in the CT-scans of specimens MCCI R775, MCCI R776 and MCCI R952, the scapula is shown as being mostly ossified instead of mostly cartilaginous, except for its dorsal margin. The scapula articulates ventrally with the coracoid bone (not reported by Andrade et al., 2016) and the paired coracoid bones flank a reduced sternum in all scanned specimens. Further support for this arrangement lies in the disarticulated specimen MDHC 427, in which a fully ossified scapula, clavicle and coracoid are present. The sternum and the interclavicle were not found in this specimen. The observed differences from the results of Andrade et al. (2016) can be interpreted as being due to the higher effectiveness and resolution of our CT-scanning and visualization methods. Moreover, having integrated the information of the CT-scans with that from disarticulated bones, we were able to provide a more complete picture of the girdle structure of this skink.

The studied material shows that the vestigial condition of the pelvic girdle is even more accentuated than that of the pectoral girdle. There is no direct contact between the ilia and the sacral vertebrae and the bones composing the pelvic girdle are undifferentiated. The ilium develops into an arch that follows the internal curvature of the body, whereas the puboischia of the two symmetric elements of the girdle do not meet at midline, being instead quite far apart. Remarkably, a very similar condition of the pelvis is present in the Malagasy mermaid skink *Voeltzkowia mobydick* (Miralles et al., 2012,

2015), which is devoid of hindlimbs similarly to *O. punctatissimus*. Also notably, both extant and extinct limbless or limb-reduced anguines display pelvic girdles in which pubis, ilium and ischium are at least partially fused (Čerňanský and Klembara, 2017), and in this regards the pelvis of *O. punctatissimus* is very similar to that of some of the extant representatives of genera like *Anguis*, *Ophisaurus* and *Pseudopus*. Differently from these anguines, *O. punctatissimus* does not have any clearly discernible suture line between the ilium and the puboischium.

Moreover, all the species included within the western species group of *Ophiomorus* (*O. latastii*, *O. persicus*, *O. punctatissimus* and, by extension, *O. kardesi*) are distinguished by the lack of connection between the transverse processes of the consecutive sacral vertebrae (the distal tip of each transverse process does not meet the respective one of the following sacral vertebra as in the standard lacertilian condition) (Greer and Wilson, 2001). This is true even in *Ophiomorus persicus*, the only species belonging to this group retaining both forelimbs and hindlimbs (Greer and Wilson, 2001). This character is clearly visible in MCCI R776 (Fig. 7), in which the transverse processes of the sacral vertebrae are widely separated, and it is further confirmed by the orientation and morphology (lack of contact surfaces) of the sacral transverse process of MDHC 427. In the other two CT-scanned specimens this character was not visible since only the skull and the first ten vertebrae were scanned.

On another note, even if in *O. punctatissimus* the pectoral girdle is much more developed than the pelvic girdle, it still shows many signs of reduction and characters that are indicated by some authors (Krieg, 1919; Stokely, 1947) as secondary symptoms of the loss of limbs. Prominently, the marked asymmetry of the girdles (as seen in Fig. 6) and the degree of morphological variation that exists between the studied specimens can both be seen as indexes of a still undergoing reduction in the pectoral region. Similar evidence of degeneration of the pectoral bones, even when the pelvic girdle is much more reduced, was highlighted by Kearney (2002) for the amphisbaenian *Bipes biporus*, which still retains its forelimbs. As in *O. punctatissimus*, *B. biporus* has very small and thin pectoral elements, and in both species the pectoral girdle is not attached to the axial skeleton.

A hypothesis regarding the asynchronous timing in the evolution of limb loss in the western species group of *Ophiomorus* could be inferred from the previously highlighted characters, as well as from the extensive literature regarding the patterns of limb reduction and loss in squamates (among others, Fürbringer, 1870; Essex, 1927; Stokely, 1947; Greer, 1991; Sanger and Gibson-Brown, 2004; Wiens, 2004; Wiens et al., 2006). Asynchronous limb loss is a very common pattern in the evolutionary path to limb reduction in squamates (Brandley et al., 2005, 2008), with the degree of forelimb regression often diverging from hindlimb regression. Among scincids, notable extreme examples of this difference in limb regression are *Lerista bipes*, in which only the hindlimbs are

retained, and the two congeneric species *Voeltzkowia mobydick* and *Voeltzkowia yamagishi*, in which on the contrary only the forelimbs are kept (Greer, 1987; Miralles et al., 2015). In *O. punctatissimus*, despite the absence of any traces of limbs, the more regressed structure of the pelvic girdle compared to that of the pectoral girdle could correspond to a matching pattern in limb reduction, in which the hindlimbs would have been lost at an evolutionarily faster pace than the forelimbs. As mentioned above, this pattern could also be present in the other western members of the genus, with the peculiar conformation of the sacral vertebrae being a common character present even in the limbed *O. persicus*, the hindlimbs of which are also greatly reduced (little more than stubs), and characterized by a lower number of digits in the pes (two) than in the manus (three) (Greer and Wilson, 2001). However, there is a significant disparity between forelimb loss and hindlimb loss in squamates, with the former being at least three times more frequent (Brandley et al., 2008). For example, snakes are known to have lost their forelimbs before their hindlimbs, as shown by the extinct genera *Eupodophis*, *Haasiophis* and *Pachyrhachis*, which still retained vestigial hindlimbs (Haas, 1979; Rage and Escuillié, 2000; Tchernov et al., 2000), and by the vestigial pelvic girdles and spurs of modern pythons and boas (Parker, 1977).

Moreover, the lack of a defined paleontological record for *O. punctatissimus*, and for the genus *Ophiomorus* as a whole, makes this theory difficult to prove apart from the direct morphological evidence. Further studies comparing the girdle anatomies of all species of *Ophiomorus* and those of other skinks and using molecular clock methods to infer the timeline of evolutionary changes are needed to gain a more in-depth understanding of the loss of limbs in this skink.

The burrowing ecomorph

Limblessness is a character that has been the focus of many studies because of its relatively high frequency in squamates (Camp, 1923; Wiens and Slingluff, 2001; Brandley et al., 2005, 2008; Wiens et al., 2006; Čerňanský, 2016). The evolution of limblessness in non-snake squamate lineages tends to be associated with one of two snakelike ecomorphs, which are the burrowing ecomorph and the grass-swimming ecomorph. These reflect differences in habitat and substrate composition (Wiens and Slingluff, 2001; Brandley et al., 2008). The burrowing ecomorph is characterized by small to nonexistent ear-openings and small eyes, body miniaturization, elongated and robust skulls that are small compared to the rest of the body, relatively short tails, short necks (keeping in mind that the cervical region and the trunk region in limbless forms are difficult to distinguish: cfr. Romer, 1956; Hoffstetter and Gasc, 1969; Čerňanský et al., 2019) and a great number of trunk vertebrae (Wiens et al., 2006; Brandley et al., 2008). It is also characterized by an enlarged vestibule in the inner ear

that almost entirely occupies the space enclosed by the semicircular canals and is interpreted as an adaptation towards the detection of low-frequency vibrations (Yi and Norell, 2015). This ecomorph, as the name suggests, reflects the adaptation to an underground life. The grass-swimming ecomorph is mainly characterized by a very long tail, which is two to 2.3 times longer than the rest of the body, and by the overall elongation of the body. Grass-swimmers derive their name from the habit of using their snakelike body shape to move quickly through grassy environments (Wiens et al., 2006).

Wiens et al. (2006) had already included *O. punctatissimus* as a representative of European skinks in their analysis, identifying it as an example of the burrowing ecomorph. The present study of the osteology of this skink confirms this conclusion, given that *O. punctatissimus* fulfills many of the diagnostic characteristics of this ecomorph: the ear openings are very small (Fig. 5); the inner ear has enlarged vestibular structures (Fig. 30; Fig. 31); the skull is twice as long as it is wide (Fig. 3; Fig. 4); the eyes are small compared to the length of the skull (Fig. 5); the number of presacral vertebrae is 53 when, according to Greer (1987), the ancestral scincid body plan comprises 26 vertebrae; the tail only represents a little less than half of the complete length of the animal (Fig. 8). Nevertheless, a difference from the diagnostic characters for burrowers, which was observed in the studied material, is the presence of autotomic vertebrae in the tail. It is stated by Wiens and Slingluff (2001) that burrowers tend to lack autotomic vertebrae because of the decreased risk of predation (although this does not represent the general rule). The condition shown in *O. punctatissimus* could be explained as the retention of a primitive lizard condition (Etheridge, 1967; LeBlanc et al., 2018) in accordance to the particular habitat in which this skink lives. Differently from most burrowing, limb-reduced skinks, *O. punctatissimus* is not usually found on sandy or loosely consolidated substrates, where burrowing would be relatively easy (Anderson and Leviton, 1966; Lymberakis et al., 2009). Instead, it lives in rocky environments, which are very common in the Peloponnese, and, as stated in the introduction, it is said to have been found in areas with sparse vegetation (Rödel et al., 1989; Lymberakis et al., 2009). Greer and Wilson (2001) also point out that the overall morphology of *O. punctatissimus* excludes it from being a sand-swimmer, suggesting instead a lifestyle on more consolidated substrates, which in fact is the predominant type of substrate found in the areas where *O. punctatissimus* lives (Anderson and Leviton, 1966). The retained capability to perform tail autotomy as a protection from predation seems to suggest that *O. punctatissimus* is subject to some form of predatory pressure, whereas a complete burrowing life habit tends to lower the risk of predation. Living in burrows and crevices among rocks suggests that, even if *O. punctatissimus* shows the morphology of the burrowing ecomorph, it is not completely secure from predation. Hence, it could be inferred that the pressure for retaining the

ability to autotomize its tail remains, but further ecological studies are needed to verify this hypothesis.

CONCLUSIONS

The results of our osteological analysis of *O. punctatissimus*, based on dry disarticulated specimens, and CT-scanned specimens, provided in-depth information regarding in particular the structure of the girdles, which are very reduced and lack any trace of vestigial limbs. The greater degree of reduction of the pelvic girdle compared to the pectoral girdle, together with the consideration that in the most phylogenetically close congeners there is a similar tendency towards the loss of hindlimbs and pelvic reduction, led us to the hypothesis that this skink lineage could have lost the hindlimbs evolutionarily earlier than the forelimbs.

Furthermore, an ecomorphological categorization of this skink was attempted based on the fact that limbless squamates tend to fall within either a burrowing ecomorph or a grass-swimming ecomorph. Based on the collected osteological and external morphological data, as well as the structure of the inner ear, we can conclude that *O. punctatissimus* clearly falls within the first category, but the presence of autotomic vertebrae in its tail suggests that, differently from most burrowers, it is subject to a noticeable predatory pressure. This could be due to the consolidated substrates on which this skink lives, which allow *O. punctatissimus* to find refuge in crevices among and under rocks, but that could still expose it to predators.

ACKNOWLEDGMENTS

We thank Gion Boano and the staff of the Museo Civico di Storia Naturale di Carmagnola for providing the specimens that were used for the CT-scans. Specimen MDHC 427 was donated by Alberto Venchi (Queensland Museum, Brisbane). Antonio Labalestra acquired the CT-scans at Microservice S.r.l. (Alpignano, Italy). Thanks are also due to Renzo Levi for the help with the digital conversions of the 3D files.

AMB was supported by National Science Foundation grant DEB-1555968 and by the Gerald M. Lemole Endowed Chair Funds.

The original map of Greece used for Fig. 2 is freely available online at d-maps.com (https://www.d-maps.com/).

The Authors declare no conflicts of interest for this publication.

AUTHORS' CONTRIBUTIONS

Concept/design: MD, AV; acquisition of data: MC, AV, MD; data analysis/interpretation: MC, AV, LCMW, AMB, ELS, MD; drafting of the manuscript: MC; critical revision of the manuscript and approval of the article: MC, AV, LCMW, AMB, ELS, MD.

REFERENCES

Anderson, S.C. and Leviton, A.E. (1966). A review of the genus *Ophiomorus* (Sauria: Scincidae), with descriptions of three new forms. Proceedings of the California Academy of Sciences, 33(16), pp. 499-534.

Andrade, J.B., Lewis, R.P. and Senter, P. (2016). Appendicular skeletons of five Asian skink species of the genera *Brachymeles* and *Ophiomorus*, including species with vestigial appendicular structures. Amphibia-Reptilia, 37(4), pp. 337–344.

Bibron, G. and Bory de Saint-Vincent, J. B. (1833). Vertébrés a Sang froid. Reptiles et Poissons. In: I. Geoffroy Saint-Hilaire and E. Geoffroy Saint-Hilaire eds., Expédition scientifique de Morée. Section des Sciences physiques. 3—1.re Partie. Zoologie. Première Section — Des animaux vertébrés, Paris and Strasbourg: F.G. Levrault, pp. 57-76.

Boulenger, G.A. (1887). Les especes du genre *Ophiomore*. Bulletin de la Societe Zoologique de France, 12, pp. 519-534.

Brandley, M.C., Schmitz, A. and Reeder, T.W. (2005). Partitioned Bayesian analyses, partition choice, and the phylogenetic relationships of scincid lizards. Systematic Biology, 54(3), pp. 373–390.

Brandley, M.C., Huelsenbeck, J.P. and Wiens J.J. (2008). Rates and patterns in the evolution of snake-like body form in squamate reptiles: evidence for repeated re-evolution of lost digits and long-term persistence of intermediate body forms. Evolution, 62(8), pp. 2042-2064.

Camp, C.L. (1923). Classification of the lizards. Bulletin of the American Museum of Natural History, 48(11), pp. 289-481.

Čerňanský, A. (2016). From lizard body form to serpentiform morphology: The atlas–axis complex in African cordyliformes and their relatives. Journal of Morphology, 277(4), pp. 512-536.

Čerňanský, A. and Klembara, J. (2017). A skeleton of *Ophisaurus* (Squamata: Anguidae) from the middle Miocene of Germany, with a revision of the partly articulated postcranial material from Slovakia using micro-computed tomography. Journal of Vertebrate Paleontology, 37(4). doi=10.1080/02724634.2017.1333515

Čerňanský, A, Yaryhin, O, Ciceková, J., Werneburg, I., Hain, M., Klembara, J. (2019). Vertebral Comparative Anatomy and Morphological Differences in Anguine Lizards With a Special Reference to *Pseudopus apodus*. The Anatomical Record, 302(2), pp. 232-257.

Duméril, A.M.C. and Bibron, G. (1839). Erpétologie générale ou Histoire naturelle complète des Reptiles, 5. Paris: Roret.

Etheridge, R. (1967). Lizard Caudal Vertebrae. Copeia, 1967(4), pp. 699-721.

Essex, R. (1927). Studies in reptilian degeneration. Proceedings of the Zoological Society of London, 97(4), pp. 879–945.

Evans, S. E. (2008). The skull of Lizards and Tuatara. In: C. Gans, A. S. Gaunt, and K. Adler, eds., Biology of the Reptilia, 20 (the Skull of Lepidosauria), Ithaca, New York. Society for the Study of Amphibians and Reptiles, Contributions to Herpetology, 23, pp. 1-347.

Fürbringer, M. (1870). Die Knochen und Muskeln der Extremitaten bei den schlangenähnlichen Sauriern. Leipzig: Verlag von Wilhelm von Engelmann.

Gelnaw, W. B. (2011). On The Cranial Osteology of *Eremiascincus* and Its Use For Identification. Electronic Theses and Dissertations, Paper 1294. http://dc.etsu.edu/etd/1294

Greer, A.E. (1986). Diagnosis of the *Lerista bipes* species-group (Lacertilia: Scincidae), with a description of a new species and an updated diagnosis of the genus. Records of the Western Australian Museum, 13(1), pp. 121-127.

Greer, A.E. (1987). Limb Reduction in the Lizard Genus *Lerista*. 1. Variation in the number of phalanges and presacral vertebrae. Journal of Herpetology, 21(4), pp. 267-276.

Greer, A.E. (1991). Limb reduction in squamates: identification of the lineages and discussion of the trends. Journal of Herpetology, 25(2), pp. 166–173.

Greer, A.E. and Wilson, G.D.F. (2001). Comments on the scincid lizard genus *Ophiomorus*, with a cladistic analysis of the species. Hamadryad, 26, pp. 261-271.

Haas, G. (1979). On a new snakelike reptile from the Lower Cenomanian of Ein Jabrud, near Jerusalem. Bulletin de le Musèe National de Histoire Naturel, 4(1), pp. 51-64.

Hermann, P., Stadler, M. (2008). Der Gesprenkelte Schlangenskink (*Ophiomorus punctatissimus* Bibron and Bory, 1833) auf der Peloponnes, Griechenland. Jahrestagung der Deutschen Gesellschaft für Herpetologie und Terrarienkunde, Karlsruhe, pp. 27-30.

Hofstetter, R. and Gasc, J.-P. (1969). Vertebrae and Ribs of Modern Reptiles. In C. Gans ed., Biology of the Reptilia, Volume I, Academic Press, New York, pp. 201-310.

Kazemi, S.M., Farhadi Qomi, M., Kami, H.G. and Anderson S.C. (2011). A new species of *Ophiomorus* (Squamata: Scincidae) from Maranjab Desert, Isfahan Province, Iran, with a revised key to the genus. Amphibian and Reptile Conservation, 5(1), pp. 23-33.

Kearney, M. (2002). Appendicular Skeleton in Amphisbaenians (Reptilia: Squamata). Copeia, 2002(3), pp. 719-738.

Kornilios, P., Kumlutaş, Y., Lymberakis, P. and Ilgaz, Ç. (2018). Cryptic diversity and molecular systematics of the Aegean *Ophiomorus* skinks (Reptilia: Squamata), with the description of a new species. Journal of Zoological Systematics and Evolutionary Research, 56(3), pp. 364-381.

Krieg, H. (1919). Beitrage zur Rudimentierungsfrage nach Beobachtungen en *Anguis fragilis*, *Chalcides tridactylus*, und *Lacerta serpa*. Archiv für Entwicklungsmechanik der Organismen, 45(4), pp. 571-601.

LeBlanc, A. R. H., MacDougall, M. J., Haridy, Y., Scott, D., & Reisz, R. R. (2017). Caudal autotomy as anti- predatory behavior in paleozoic reptiles. Scientific Reports, 8(1). https://doi.org/10.1038/s41598-018-21526-3

Lymberakis, P., Tok, V., Ugurtas et al. (2009). *Ophiomorus punctatissimus*. IUCN Red List of Threatened Species 2009 [online]. https://www.iucnredlist.org. Available at: http://dx.doi.org/10.2305/IUCN.UK.2009.RLTS.T61540A12511332.en [Accessed 18 March 2018].

Miralles, A., Anjeriniaina, M., Hipsley, C.A., Müller, J., Glaw, F. and Vences M. (2012). Variations on a bauplan: description of a new Malagasy "mermaid skink" with flipper-like forelimbs only (Scincidae, *Sirenoscincus* Sakata and Hikida, 2003). Zoosystema, 34(4), pp. 701-719.

Miralles, A., Hipsley, C.A., Erens, J. et al. (2015). Distinct patterns of desynchronized limb regression in Malagasy scincine lizards (Squamata, Scincidae). PLoS ONE, 10(6), e0126074.

Nilson, G. and Andrén, C. (1978). A new species of *Ophiomorus* (Sauria: Scincidae) from Kavir Desert, Iran. Copeia, 1978(4), pp. 559-564.

Paluh, D.J. and Bauer, A.M. (2017). Comparative skull anatomy of terrestrial and crevice-dwelling *Trachylepis* skinks (Squamata: Scincidae) with a survey of resources in scincid cranial osteology. PLoS ONE, 12(9), e0184414.

Parker, H.W. (1977). Snakes, a Natural History. Brisbane: University of Queensland Press.

Poulakakis, N., Pakaki, V., Mylonas, M. and Lymberakis, P. (2008). Molecular phylogeny of the Greek legless skink *Ophiomorus punctatissimus* (Squamata: Scincidae): The impact of the Mid-Aegean trench in its phylogeography. Molecular Phylogenetics and Evolution, 47, pp. 396–402.

Rage, J.C. and Augé, M. (2010). Squamate reptiles from the middle Eocene of Lissieu (France). A landmark in the middle Eocene of Europe. Geobios, 43, pp. 253–268.

Rage, J.C. and Escuillié, F. (2000). Un nouveau serpent bipède du Cénomanien (Crétacé). Implications phylétiques. Comptes Rendus de l'Académie des Sciences, Earth Sciences, 330, pp. 513–520.

Rödel, M.-O., Bussmann, R. and Kaupp, A. (1989). Beitrag zur Biotopwahl von *Ophiomorus punctatissimus* (Bibron and Bory 1833). Sauria 11(1), pp. 27-30.

Romer, A.S. (1956). Osteology of the Reptiles. Chicago: University of Chicago Press.

Russell, A.P. and Bauer, A.M. (2009). The appendicular locomotor apparatus of *Sphenodon* and normal-limbed squamates. In: C. Gans, A.S. Gaunt and K. Adler eds., Biology of the Reptilia, 21 (Morphology I), Ithaca, New York: Society for the Study of Amphibians and Reptiles, pp. 1-465.

Sanger, T.J. and Gibson-Brown J.J. (2004). The developmental bases of limb reduction and body elongation in squamates. Evolution, 58(9), pp. 2103-2106.

Siler, C. D., Brown, R. M. (2011). Evidence for repeated acquisition and loss of complex body- form characters in an insular clade of Southeast Asian semi- fossorial skinks. Evolution, 65(9), pp. 2641–2663.

Speybroeck, J, Beukema, W, Bok, B, Van Der Voort, J, Velikov, I. (2016). Field guide to the amphibians and reptiles of Britain and Europe. London: Bloomsbury.

Stokely, P. S. (1947). Limblessness and correlated changes in the girdles of a comparative morphological series of lizards. American Midland Naturalist, 38(3), pp. 725-754.

Tchernov, E., Rieppel, O., Zaher, H., Polcyn, M.J. and Jacobs, L.L. (2000). A fossil snake with limbs. Science, 287(5460), pp. 2010-2012.

Townsend, V.R. Jr., Akin, J.A., Felgenhauer, B.E., Dauphine, J. and Kidder, S.A. (1999). Dentition of the ground skink, *Scincella lateralis* (Sauria, Scincidae). Copeia, 3, pp. 783-788.

Tschopp, E. (2016). Nomenclature of vertebral laminae in lizards, with comments on ontogenetic and serial variation in lacertini (Squamata, Lacertidae). PLoS ONE, 11(2), e0149445.

Wiens, J.J. (2004). Development and evolution of body form and limb reduction in squamates: a response to Sanger and Gibson-Brown. Evolution, 58(9), pp. 2107-2108.

Wiens, J.J., Brandley, M.C. and Reeder, T.W. (2006). Why does a trait evolve multiple times within a clade? Repeated evolution of snakelike body form in squamate reptiles. Evolution, 60(1), pp. 123–141.

Wiens, J.J. and Slingluff, J.L. (2001). How lizards turn into snakes: a phylogenetic analysis of body-form evolution in anguid lizards. Evolution 55(11), pp. 2303–2318.

Yi, H., Norell, M. A. (2015). The burrowing origin of modern snakes. Science Advances, 1(10), e1500743.

FIGURE LEGENDS

FIGURE LEGENDS

Figure 1. *Ophiomorus punctatissimus* from the Peloponnese. Photo by Benny Trapp.

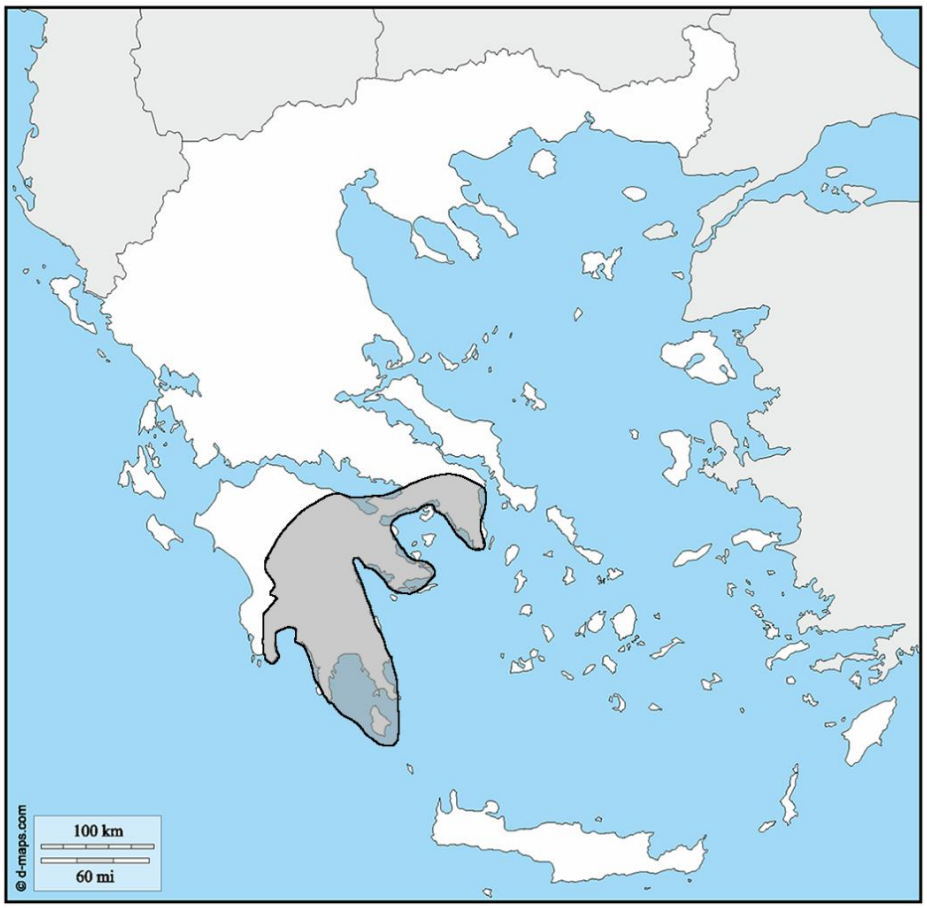

Figure 2. Geographic distribution of *O. punctatissimus* in Greece, based on the data reported by Poulakakis et al. (2008).

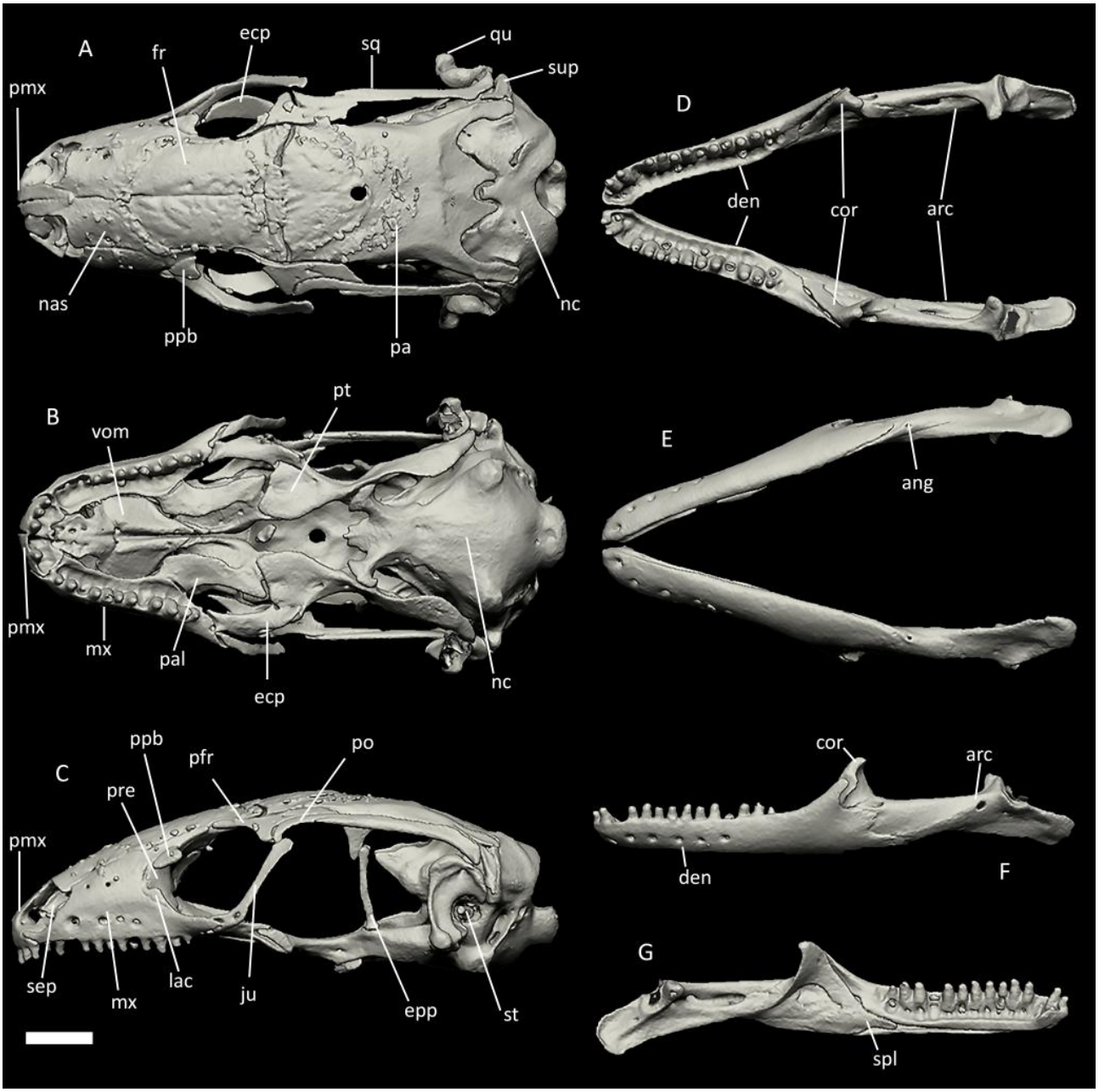

Figure 3. CT-scan of the skull of *O. punctatissimus* MCCI R776 (visualized with Zbrush 4R8). A: cranium, dorsal view; B: cranium, ventral view; C: cranium, left lateral view; D: mandibles, dorsal view; E: mandibles, ventral view; F: left mandible, lateral view; G: left mandible, medial view. The osteoderm cover was almost completely removed digitally. Abbreviations: ang: angular; arc: articular complex; cor: coronoid; den: dentary; ecp: ectopterygoid; epp: epipterygoid; fr: frontal; ju: jugal; mx: maxilla; lac: lacrimal; nas: nasal; nc: neurocranium; pa: parietal; pal: palatine; pfr: postfrontal; pmx: premaxilla; po: postorbital; ppb: palpebral; pre: prefrontal; pt: pterygoid; qu: quadrate; sep: septomaxilla; spl: splenial; sq: squamosal; st: stapes; sup: supratemporal; vom: vomer. Scale bar: 1 mm.

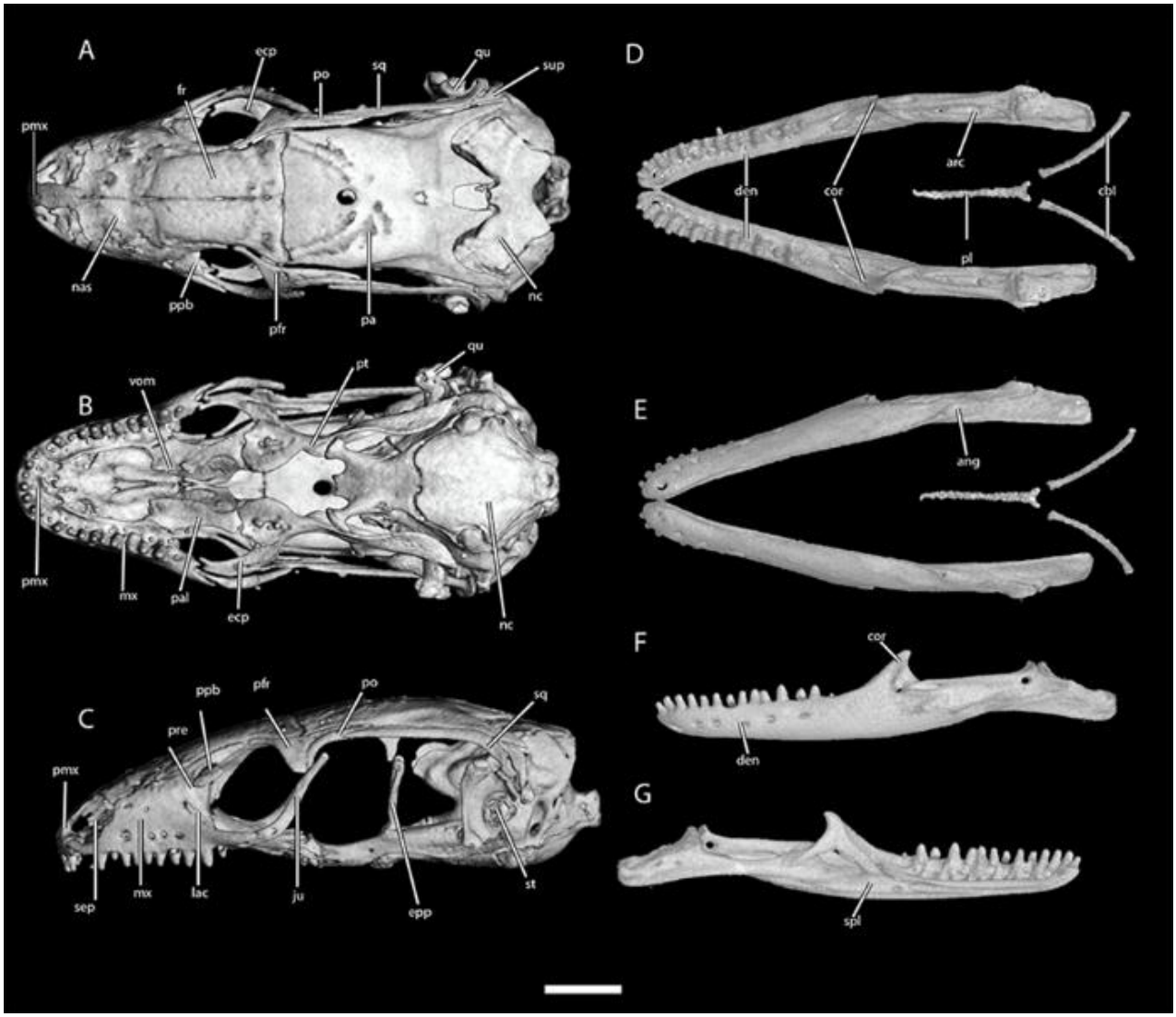

Figure 4. CT-scan of the skull of *O. punctatissimus* MCCI R775 (visualized with VGStudioMax 3.2.2). A: cranium, dorsal view; B: cranium, ventral view; C: cranium, left lateral view; D: mandibles, dorsal view; E: mandibles, ventral view; F: left mandible, lateral view; G: left mandible, medial view. The osteoderm cover was almost completely removed digitally. Abbreviations: ang: angular; arc: articular complex; cbl: ceratobranchials; cor: coronoid; den: dentary; ecp: ectopterygoid; epp: epipterygoid; fr: frontal; ju: jugal; mx: maxilla; lac: lacrimal; nas: nasal; nc: neurocranium; pa: parietal; pal: palatine; pfr: postfrontal; pl: processus lingualis; pmx: premaxilla; po: postorbital; ppb: palpebral; pre: prefrontal; pt: pterygoid; qu: quadrate; sep: septomaxilla; spl: splenial; sq: squamosal; st: stapes; sup: supratemporal; vom: vomer. Scale bar: 1 mm.

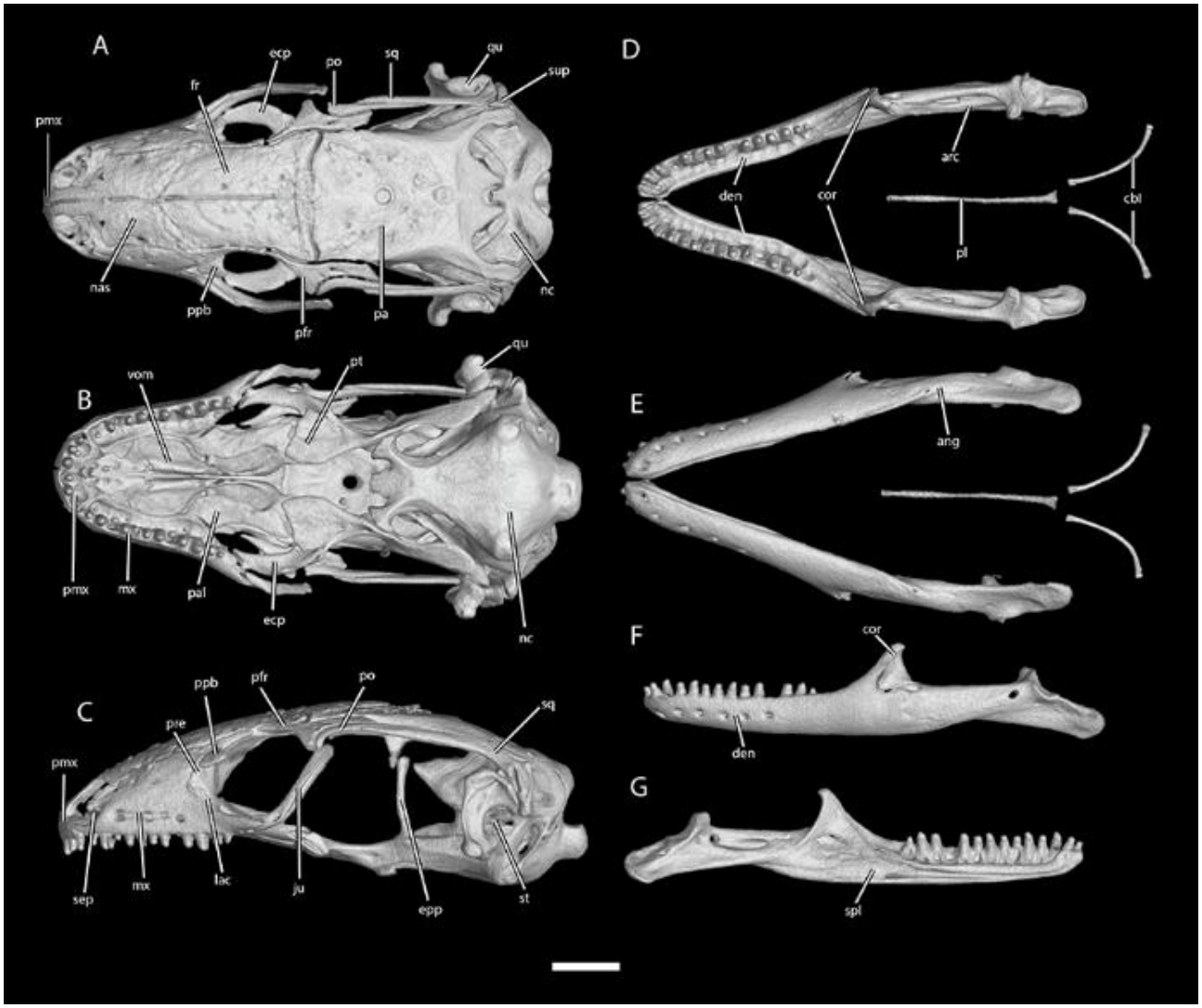

Figure 5. CT-scan of the skull of *O. punctatissimus* MCCI R952 (visualized with VGStudioMax 3.2.2). A: cranium, dorsal view; B: cranium, ventral view; C: cranium, left lateral view; D: mandibles, dorsal view; E: mandibles, ventral view; F: left mandible, lateral view; G: left mandible, medial view. The osteoderm cover was almost completely removed digitally. Abbreviations: ang: angular; arc: articular complex; cbl: ceratobranchials; cor: coronoid; den: dentary; ecp: ectopterygoid; epp: epipterygoid; fr: frontal; ju: jugal; mx: maxilla; lac: lacrimal; nas: nasal; nc: neurocranium; pa: parietal; pal: palatine; pfr: postfrontal; pl: processus lingualis; pmx: premaxilla; po: postorbital; ppb: palpebral; pre: prefrontal; pt: pterygoid; qu: quadrate; sep: septomaxilla; spl: splenial; sq: squamosal; st: stapes; sup: supratemporal; vom: vomer. Scale bar: 1 mm.

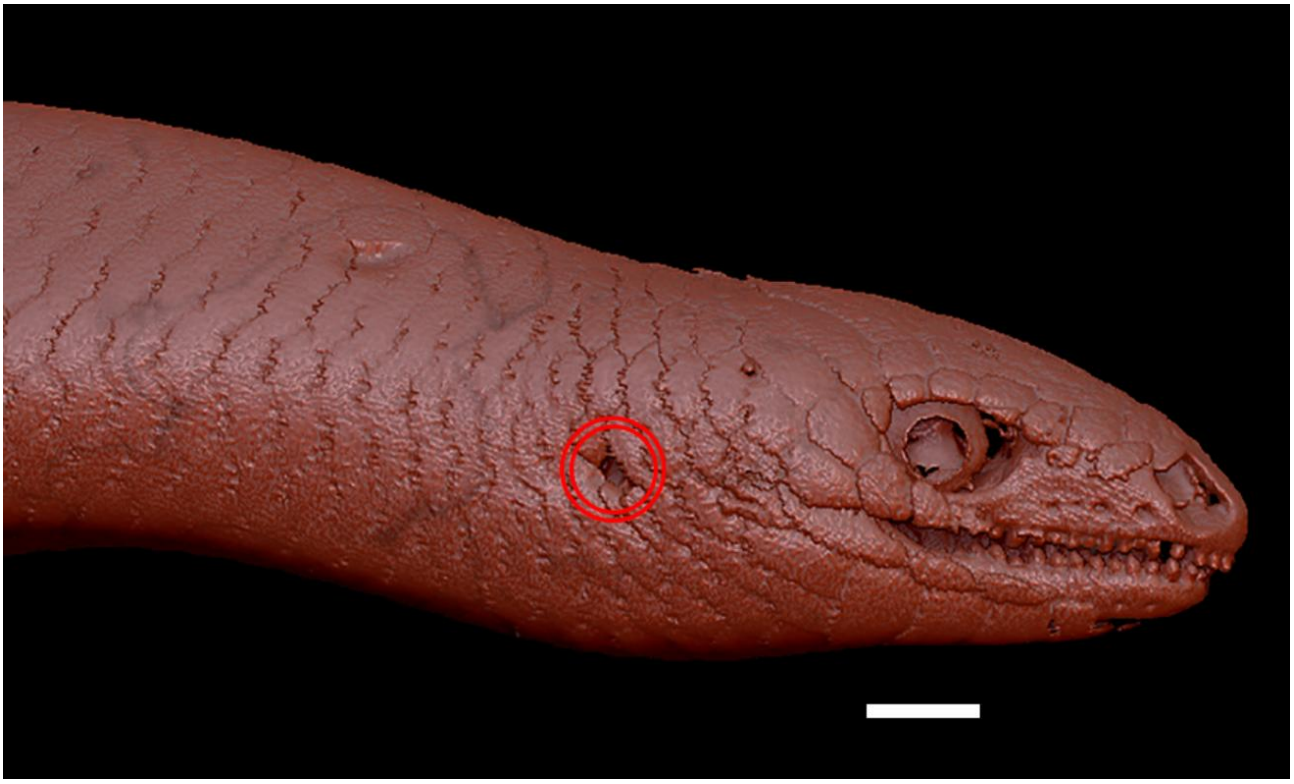

Figure 6. Right lateral view of the head and the anterior portion of the trunk of *O*. *punctatissimus* MCCI R775 (visualized with Zbrush 4R8). The two red circles indicate the position of the ear opening. Scale bar: 1 mm.

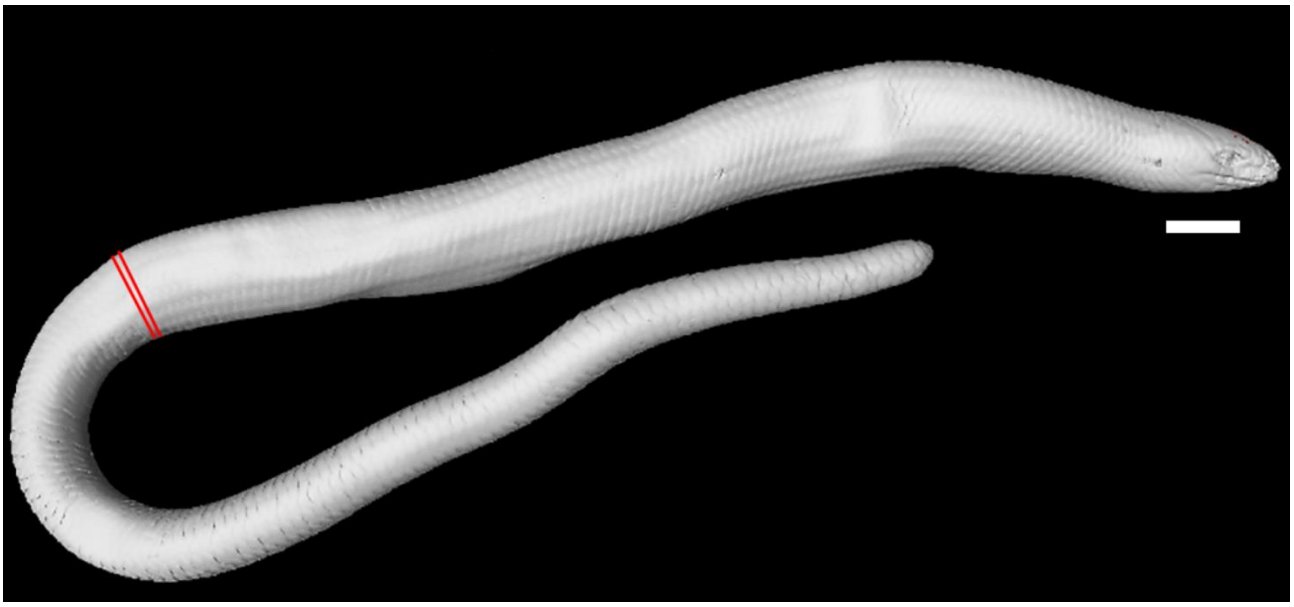

Figure 7. Right lateral view of the full CT-scan of *O*. *punctatissimus* MCCI R776 (visualized with myVGL 3.0). Red markings indicate the beginning of the tail. Scale bar: 5 mm.

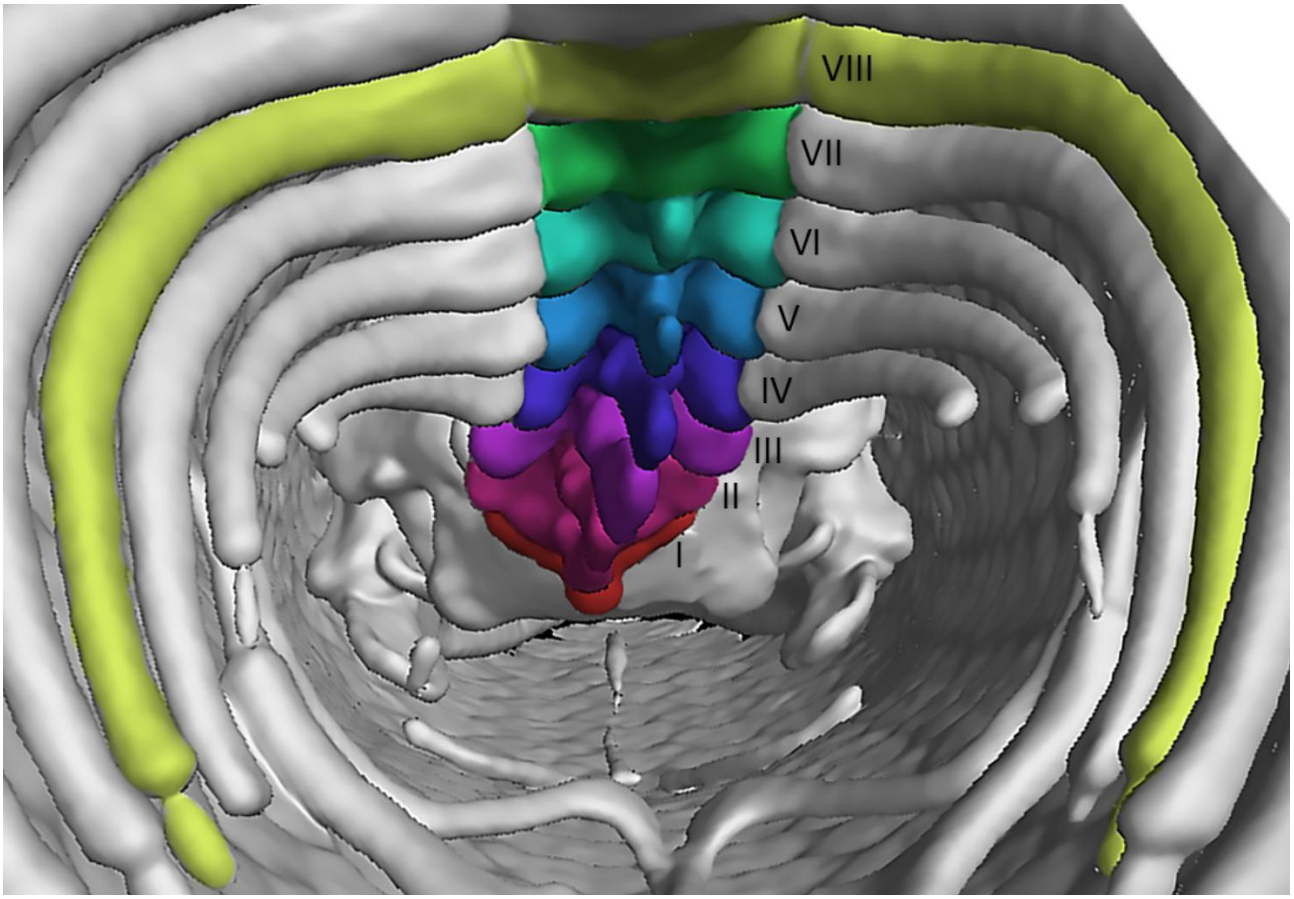

Figure 8. Anterior portion of the trunk cavity of *O. punctatissimus* MCCI R776 in posterior view, showing the cervical vertebrae (visualized with myVGL 3.0). The seven cervical elements were numbered and colored (see the online version of the article) in order to be easily distinguishable. Following Hoffstetter and Gasc (1969), the eighth vertebra (VIII) is here considered as the first trunk vertebra because the ribs to which it articulates are connected to the sternum (st) through the associated sternal ribs. Scale bar: 1 mm.

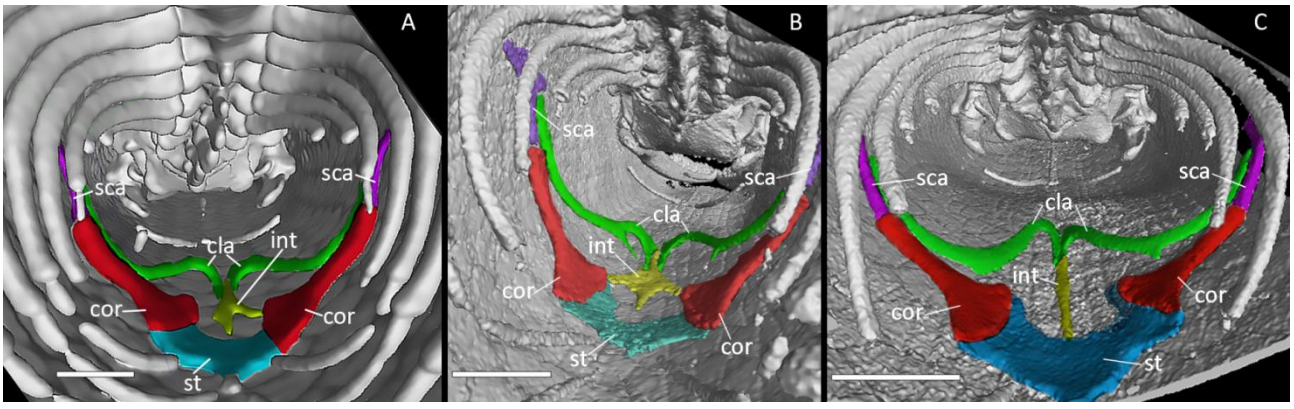

Figure 9. Anterior portion of the trunk cavities of three specimens of *O. punctatissimus* in posterior view, showing the pectoral girdle (visualized with myVGL 3.0, colorized). A: MCCI R776; B: MCCI R775; C: MCCI R952. Abbreviations: cor: coracoids (red); st: sternum (blue); int: interclavicle (yellow); cla: clavicles (green); sca: scapulae (purple). Scale bars: 1 mm.

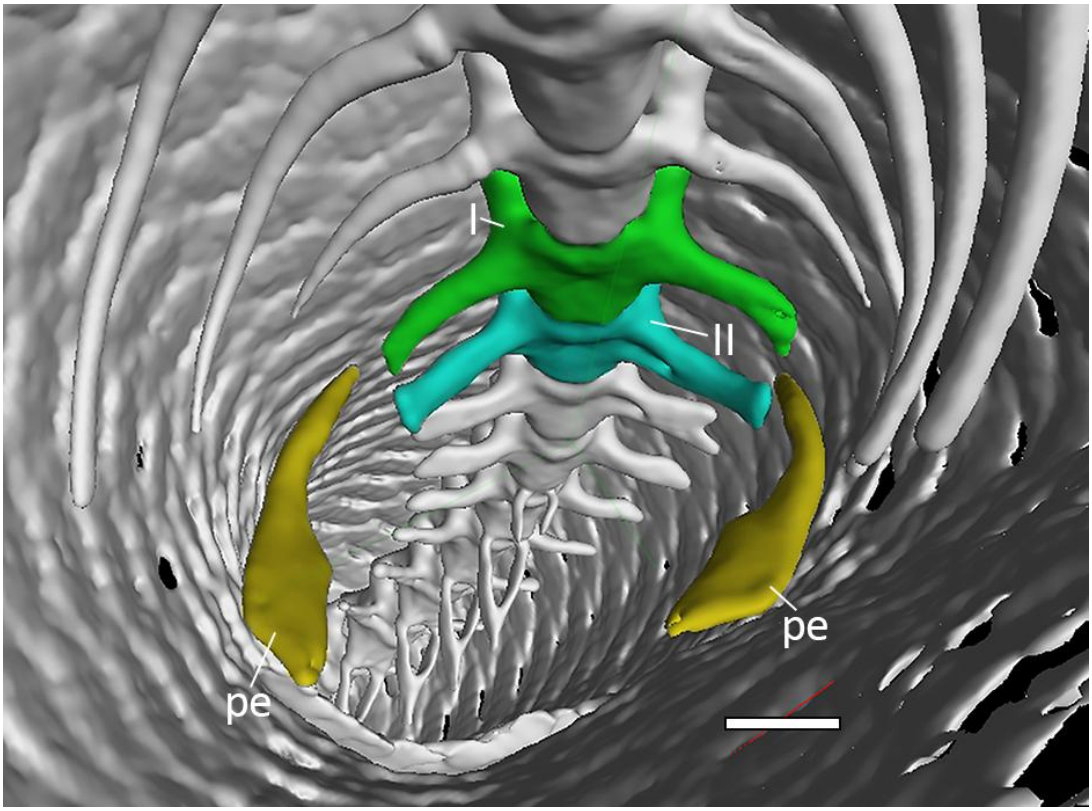

Figure 10. Posterior portion of the trunk cavity of *O*. *punctatissimus* MCCI R776 in anterior view, showing the sacral vertebrae and the pelvic girdle (visualized with myVGL 3.0, colorized). Abbreviations: I: sacral vertebra I (green); II: sacral vertebra II (blue); pe: pelvic elements (yellow). Scale bar: 1 mm.

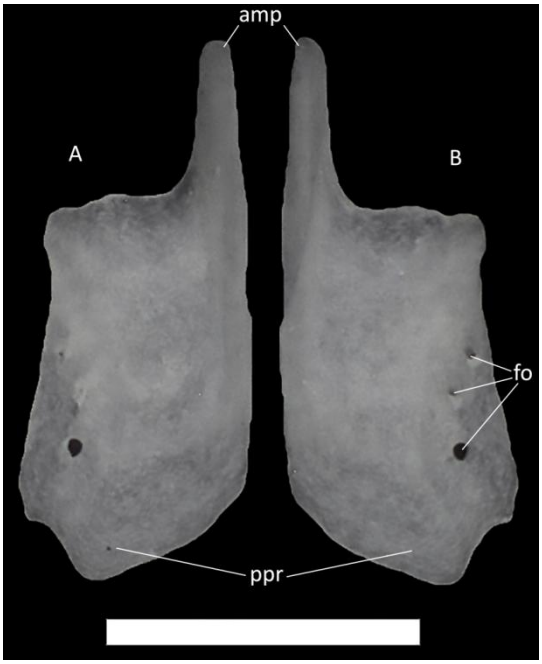

Figure 11. *Ophiomorus punctatissimus* MDHC 427, right nasal. A: ventral view; B: dorsal view. Abbreviations: amp: anteromedial process; fo: formina; ppr: posterior process. Scale bar: 1 mm.

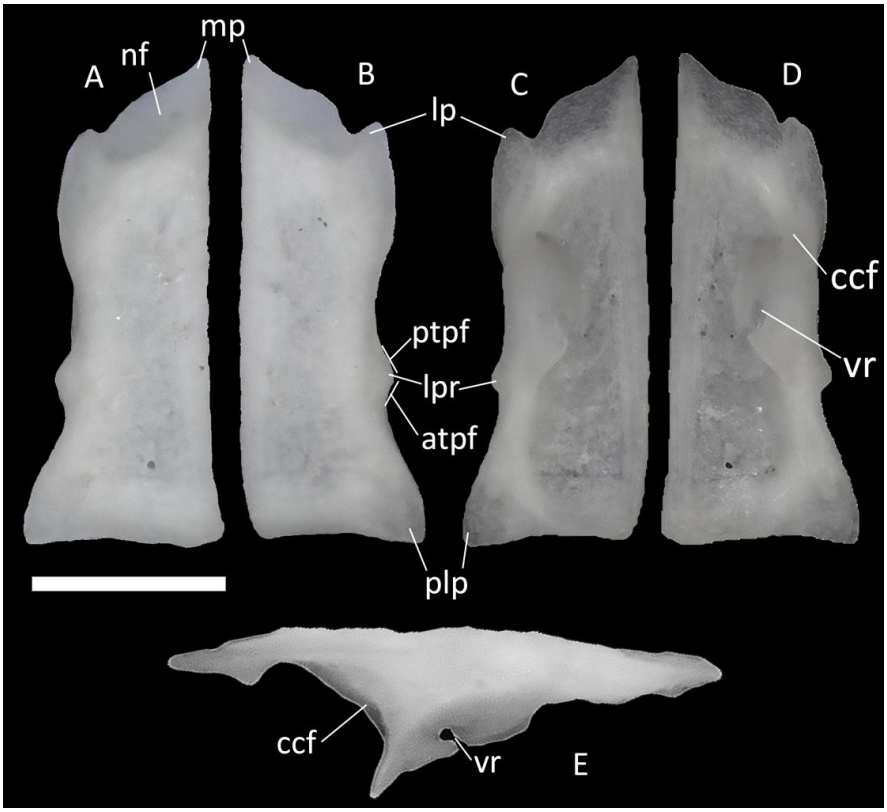

Figure 12. *Ophiomorus punctatissimus* MDHC 427, left (A, C, E) and right (B, D) frontals. A, B: dorsal view; C, D: ventral view; E; lateral view. Abbreviations: atpf: anterior end of the postfrontal facet; ccf: crista cranii frontalis; lp: lateral process; lpr: lateral projection; mp: medial process; nf: nasal facet; plp: posterolateral process; ptpf: posterior end of the prefrontal facet; vr: ventral recess. Scale bar: 1 mm.

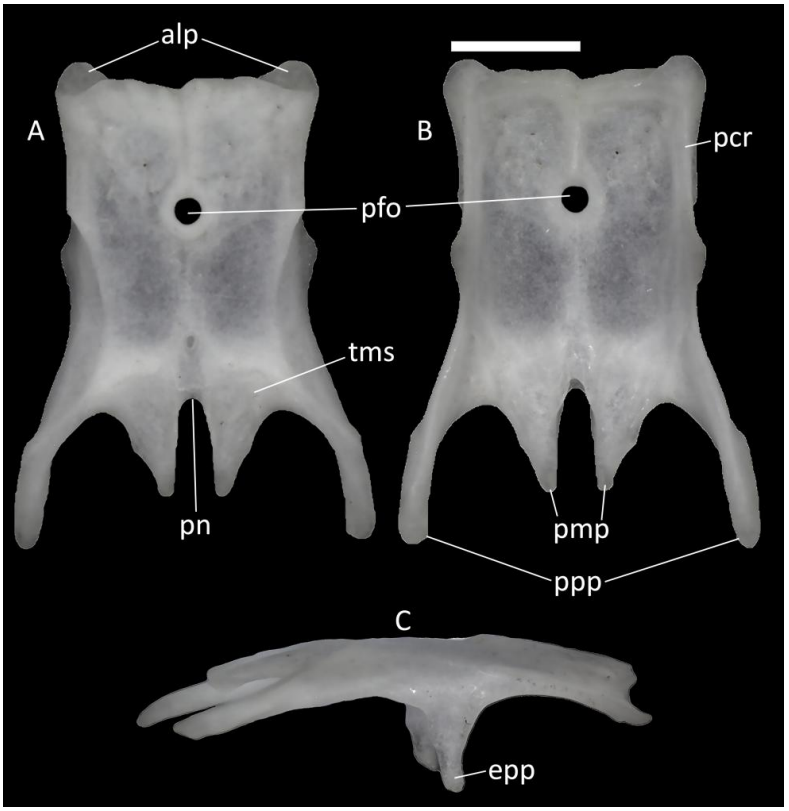

Figure 13. *Ophiomorus punctatissimus* MDHC 427, parietal. A: dorsal view; B: ventral view; C: right lateral view. Abbreviations: alp: anterolateral process; epp: epipterygoid process; pcr: parietal crest; pfo: parietal

foramen; pmp: posteromedial process; pn: parietal notch; ppp: postparietal process; tms: temporal muscle scar. Scale bar: 1 mm.

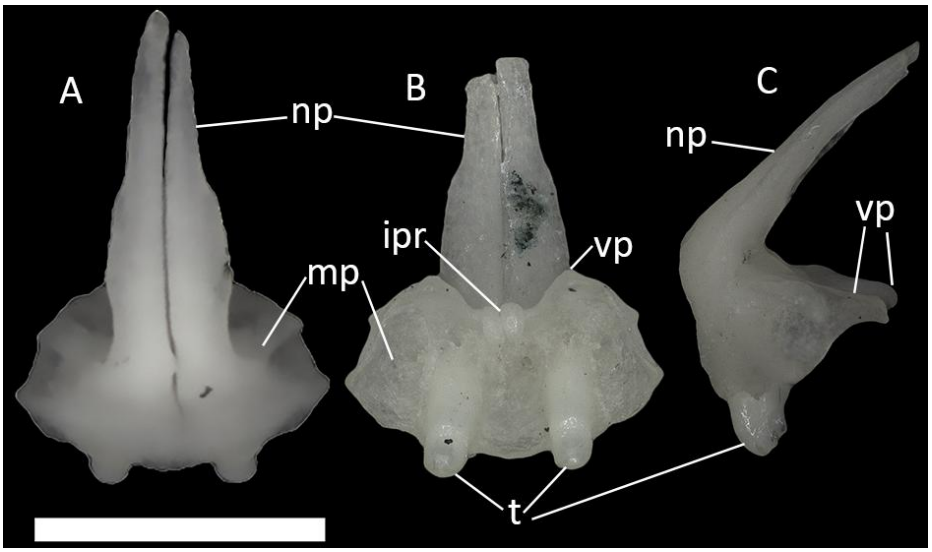

Figure 14. *Ophiomorus punctatissimus* MDHC 427, partially fused premaxillae. A: dorsal view; B: ventral view; C: left lateral view. Abbreviations: ipr: incisive process; np: nasal process; mp: maxillary process; t: teeth; vp: vomerine process. The distal end of the nasal process in Figures B and C broke during manipulation. Scale bar: 1 mm.

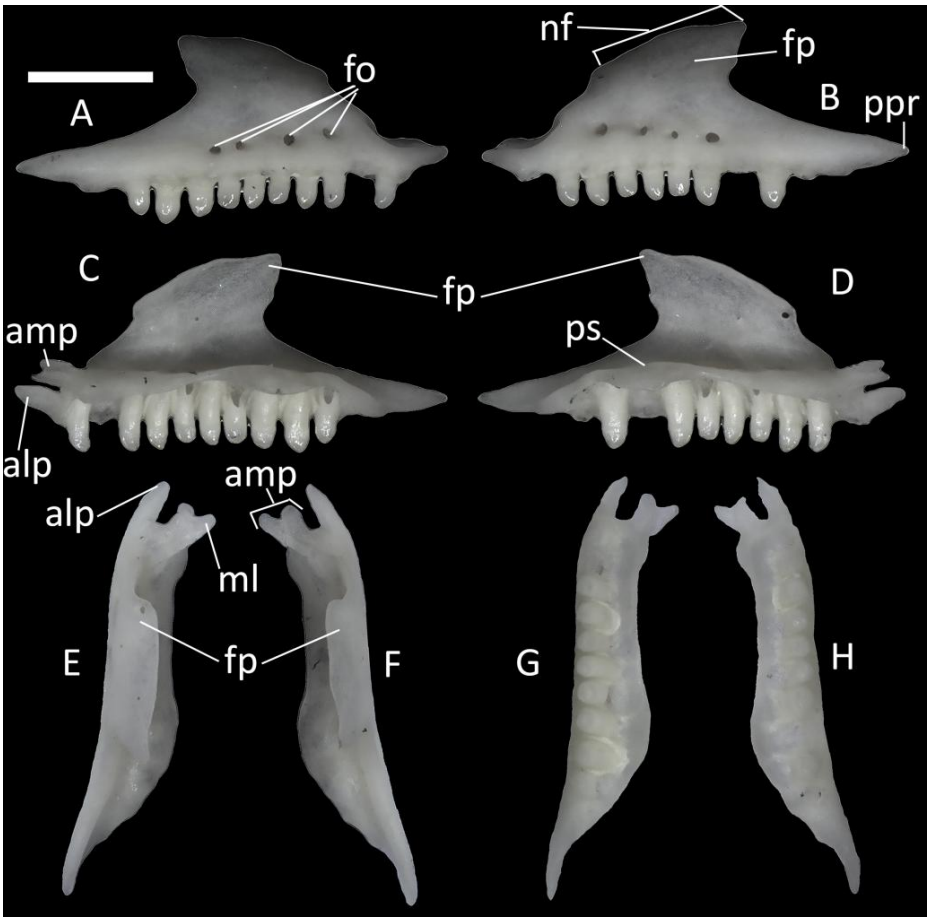

Figure 15. *Ophiomorus punctatissimus* MDHC 427, right (A, C, E, G) and left (B, D, F, H) maxillae. A, B: lateral view; C, D: medial view; E, F; dorsal view; G, H: ventral view. Abbreviations: alp: anterolateral process; amp:

anteromedial process; fo: foramina; fp: facial process; ml: medial lappet; nf: nasal facet; ppr: posterior process; ps: palatal shelf. Scale bar: 1 mm.

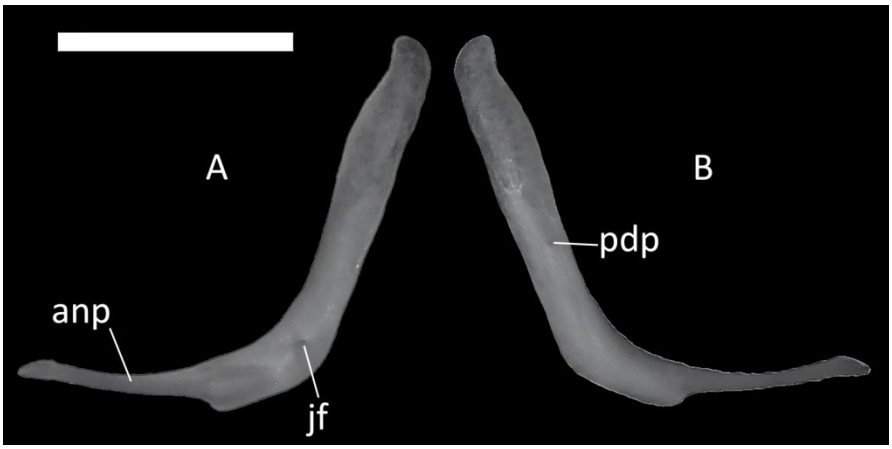

Figure 16. *Ophiomorus punctatissimus* MDHC 427, left jugal. A: lateral view; B: medial view. Abbreviations: anp: anterior process; jf: jugal foramen; pdp: posterodorsal process. Scale bar: 1 mm.

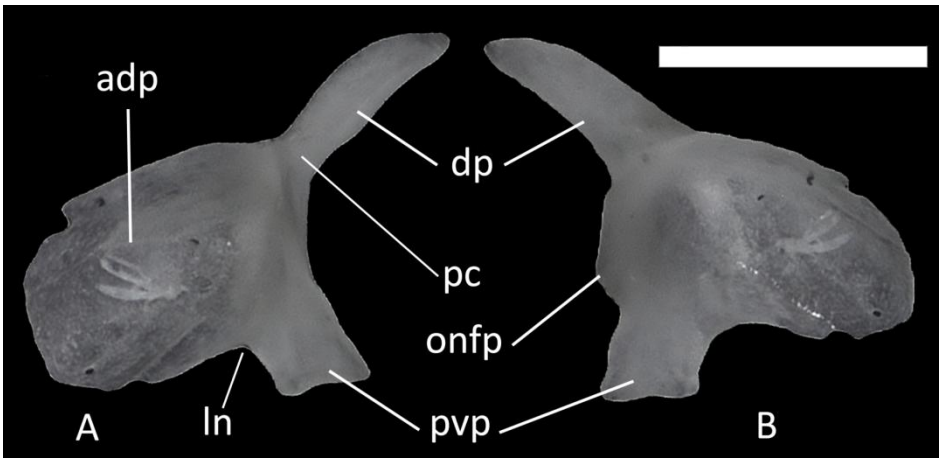

Figure 17. *Ophiomorus punctatissimus* MDHC 427, left prefrontal. A: lateral view; B: medial view. Abbreviations: adp: anterodorsal process; dp: dorsal process; ln: lacrimal notch; pc: palpebral crest; pvp: posteroventral process; onfp: orbitonasal flange projection. Scale bar: 1 mm.

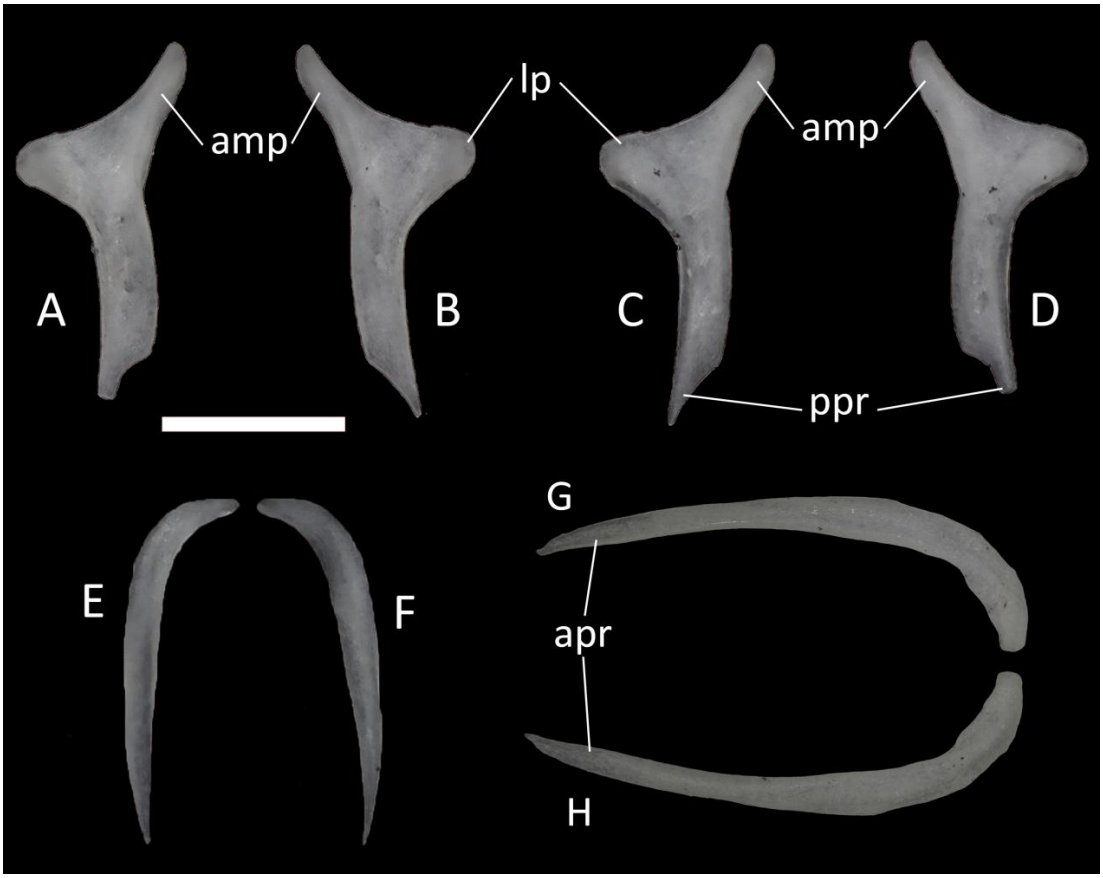

Figure 18. *Ophiomorus punctatissimus* MDHC 427, left (A, D) and right (B, C) postfrontals, left postorbital (E, F) and right squamosal (G, H). A, B, E, H: dorsal view; C, D, F, G: ventral view. Abbreviations: amp: anteromedial process; apr: anterior process; lp: lateral process; ppr: posterior process. Scale bar: 1 mm.

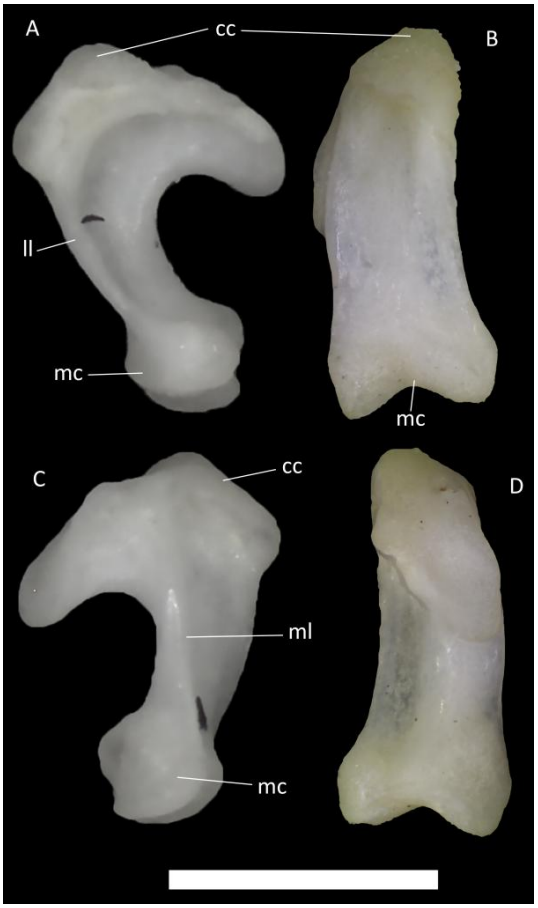

Figure 19. *Ophiomorus punctatissimus* MDHC 427, left quadrate. A: lateral view; B: anterior view; C: medial view; D: posterior view. Abbreviations: cc: cephalic condyle; ll: lateral lamina; mc: mandibular condyle; ml: medial lamina. Scale bar: 1 mm.

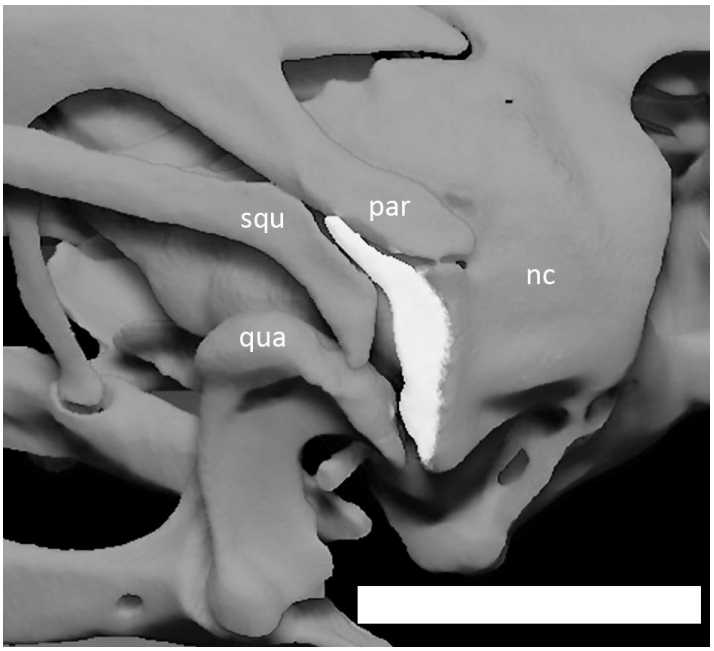

Figure 20. Left supratemporal (in white) of *O. punctatissimus* MCCI R776, in posterolateral view (visualized with Zbrush 4R8). Abbreviations: nc: neurocranium; par: parietal; qua: quadrate; squ: squamosal. Scale bar: 1 mm.

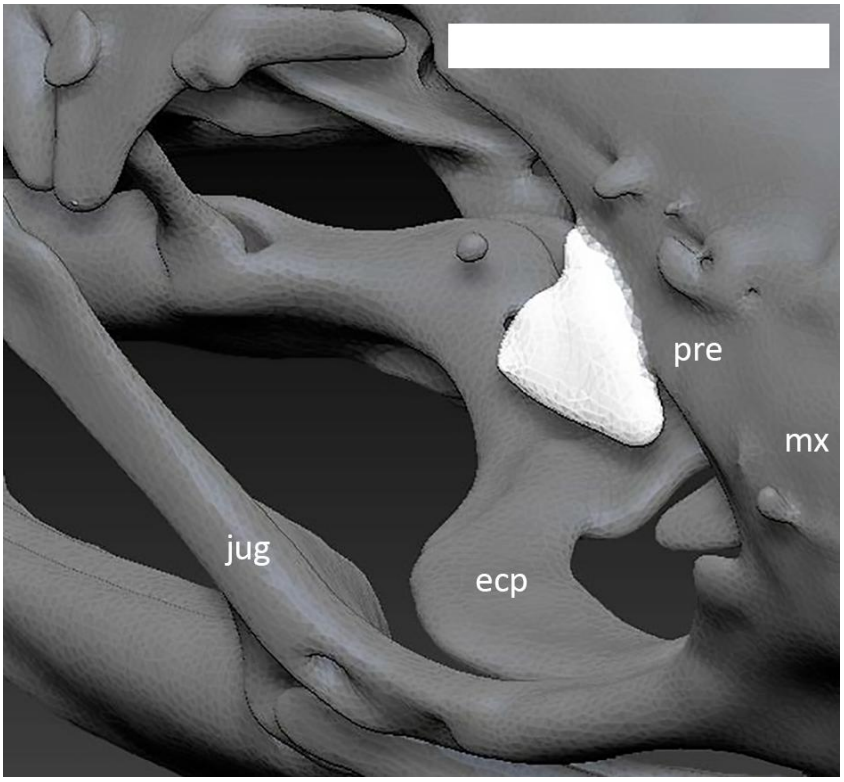

Figure 21. Right palpebral (in white) of *O*. *punctatissimus* MCCI R776, in anterodorsal view (visualized with Zbrush 4R8). Abbreviations: ecp: ectopterygoid; jug: jugal; mx: maxilla; pre: prefrontal. Scale bar: 1 mm.

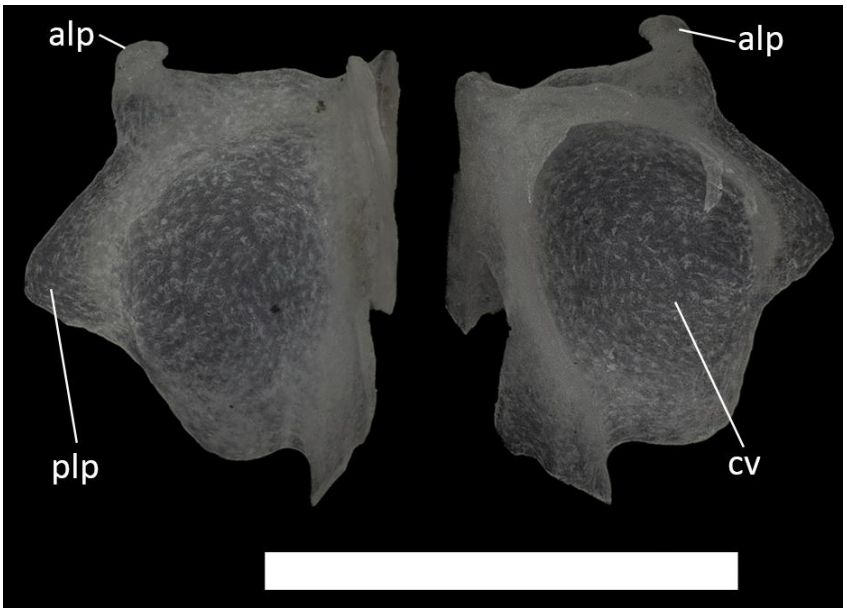

Figure 22. *Ophiomorus punctatissimus* MDHC 427, left septomaxilla. A: dorsal view; B: ventral view. Abbreviations: alp: anterolateral process; cv: concha vomeronasalis; plp: posterolateral process. Scale bar: 1 mm.

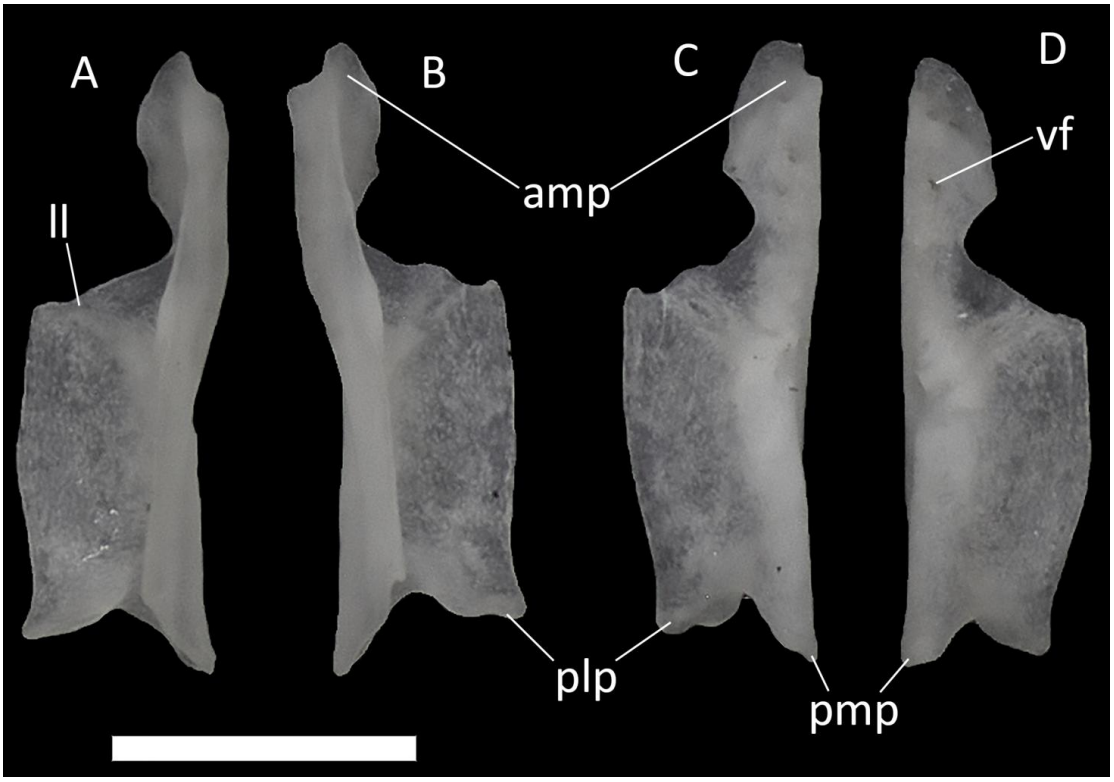

Figure 23. *Ophiomorus punctatissimus* MDHC 427, left (A, D) and right (B, C) vomers. A, B: dorsal view; C, D: ventral view. Abbreviations: amp: anteromedial process; ll: lateral lamina; plp: posterolateral process; pmp: posteromedial process; vf: vomerine foramen. Scale bar: 1 mm.

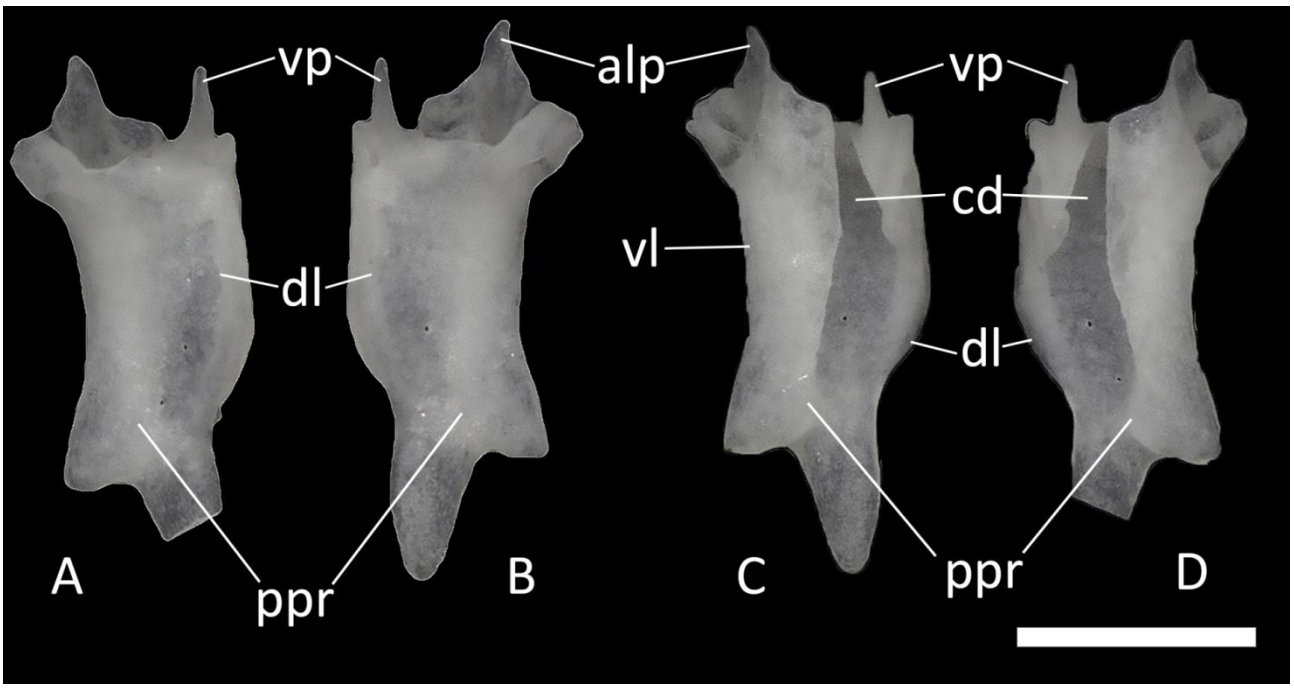

Figure 24. *Ophiomorus punctatissimus* MDHC 427, left (A, D) and right (B, C) palatines. A, B: dorsal view; C, D: ventral view. Abbreviations: alp: anterolateral process; cd: choanal duct; dl: dorsal lamina; ecp: ectopterygoid process; ppr: pterygoid process; vl: ventral lamina; vp: vomerine process. In the left palatine, the tip of the posterior extension of the pterygoid process is broken off. Scale bar: 1 mm.

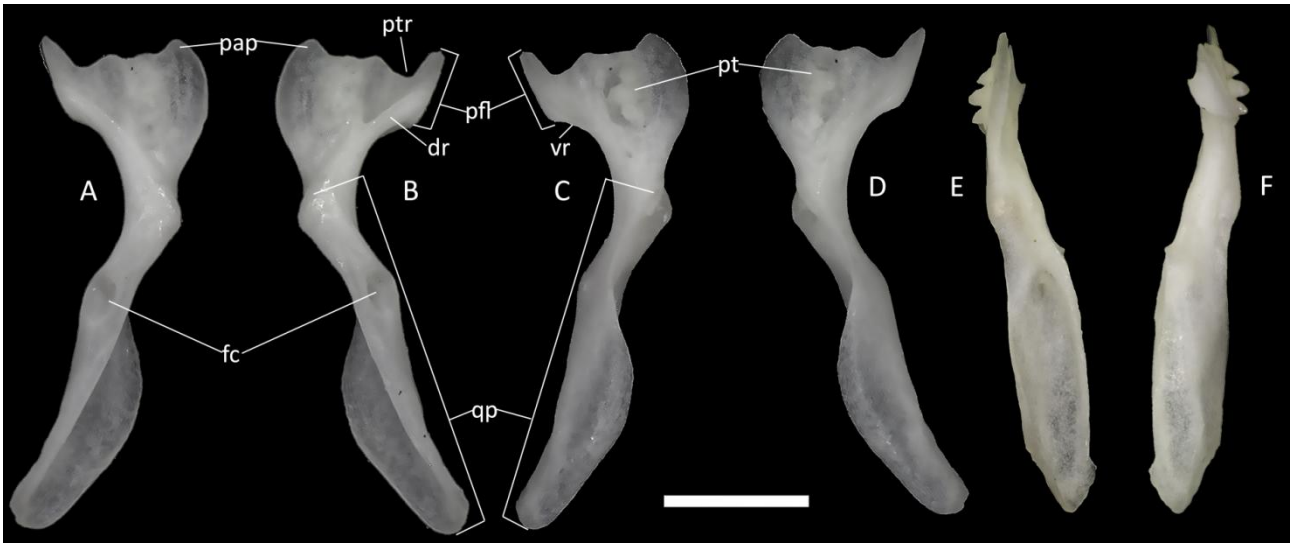

Figure 25. *Ophiomorus punctatissimus* MDHC 427, left (A, D) and right (B, C, E, F) pterygoids. A, B: dorsal view; C, D: ventral view; E: medial view; F: lateral view. Abbreviations: dr: dorsal ridge; fc: fossa columellae; pap: palatine process; pfl: pterygoid flange; pt: pterygoid teeth; ptr: pterygoid recess; qp: quadrate process; vr: ventral ridge. Scale bar: 1 mm.

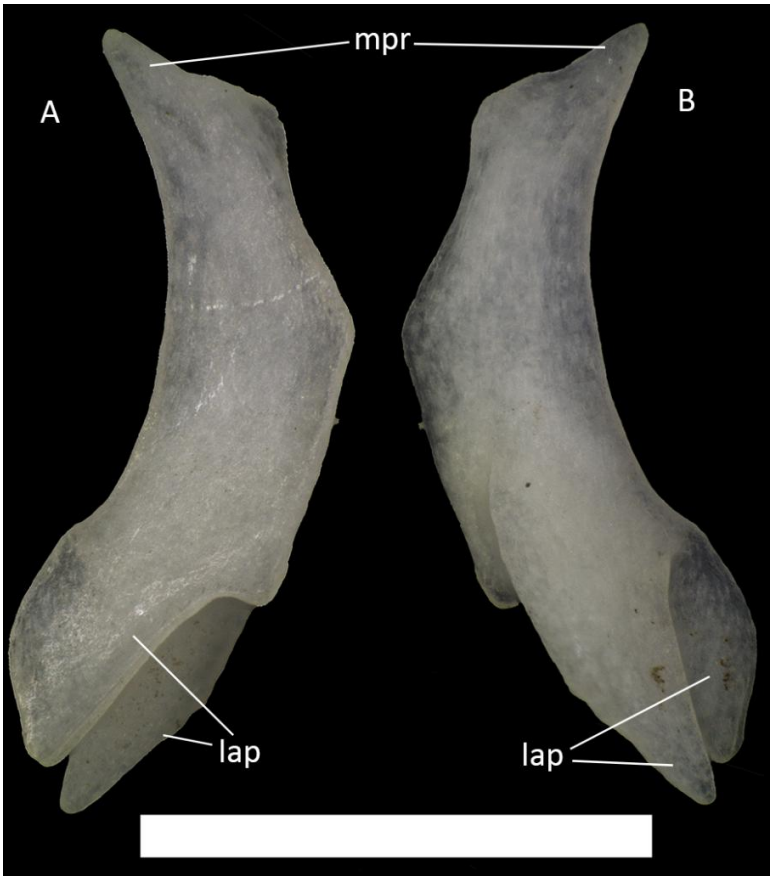

Figure 26. *Ophiomorus punctatissimus* MDHC 427, left ectopterygoid. A: dorsal view; B: ventral view. Abbreviations: mpr: maxillary process; lap: lappets. Scale bar: 1 mm.

Figure 27. *Ophiomorus punctatissimus* MDHC 427, left epipterygoid in lateral view. Scale bar: 1 mm.

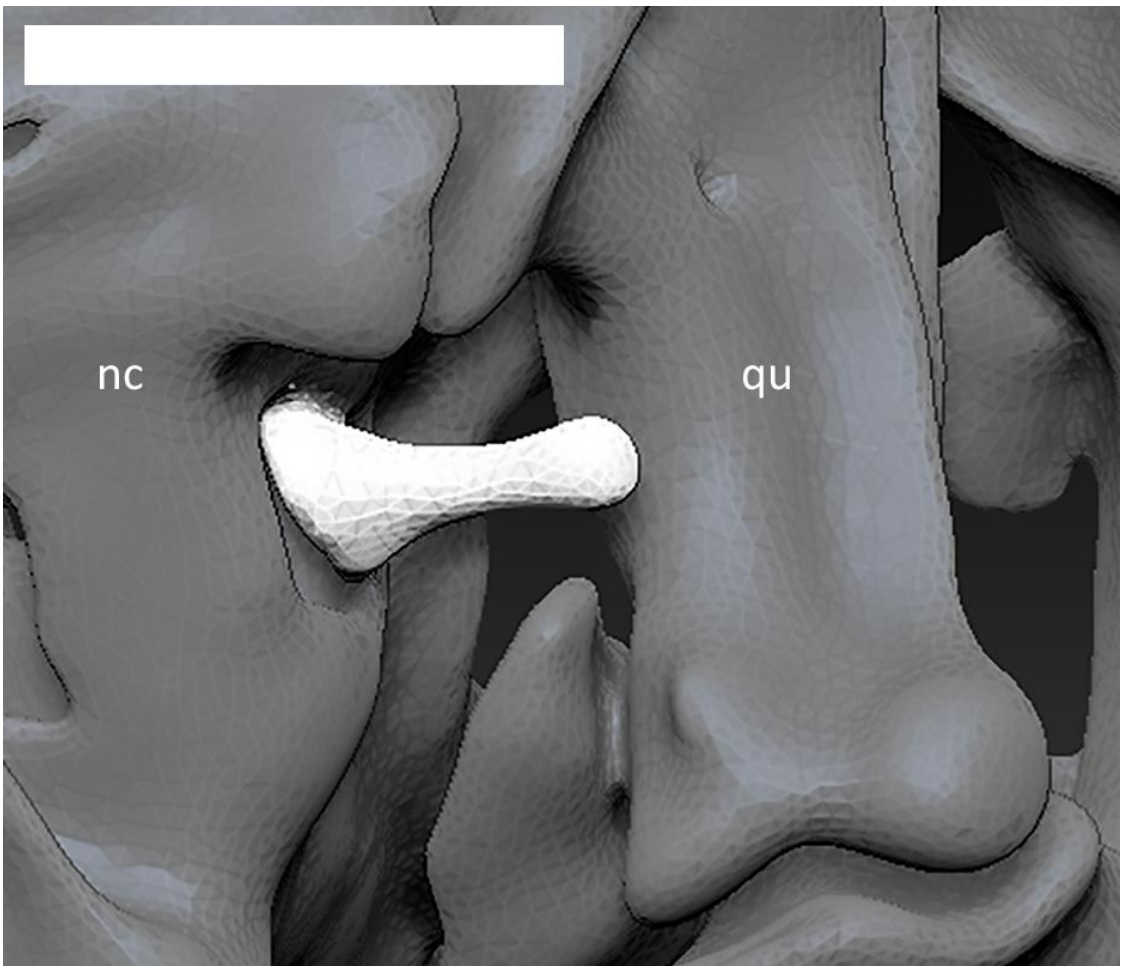

Figure 28. Right stapes (in white) of *O*. *punctatissimus* MCCI R776, in posterior view (visualized with Zbrush 4R8). Abbreviations: nc: neurocranium; qu: quadrate. Scale bar: 0.5 mm.

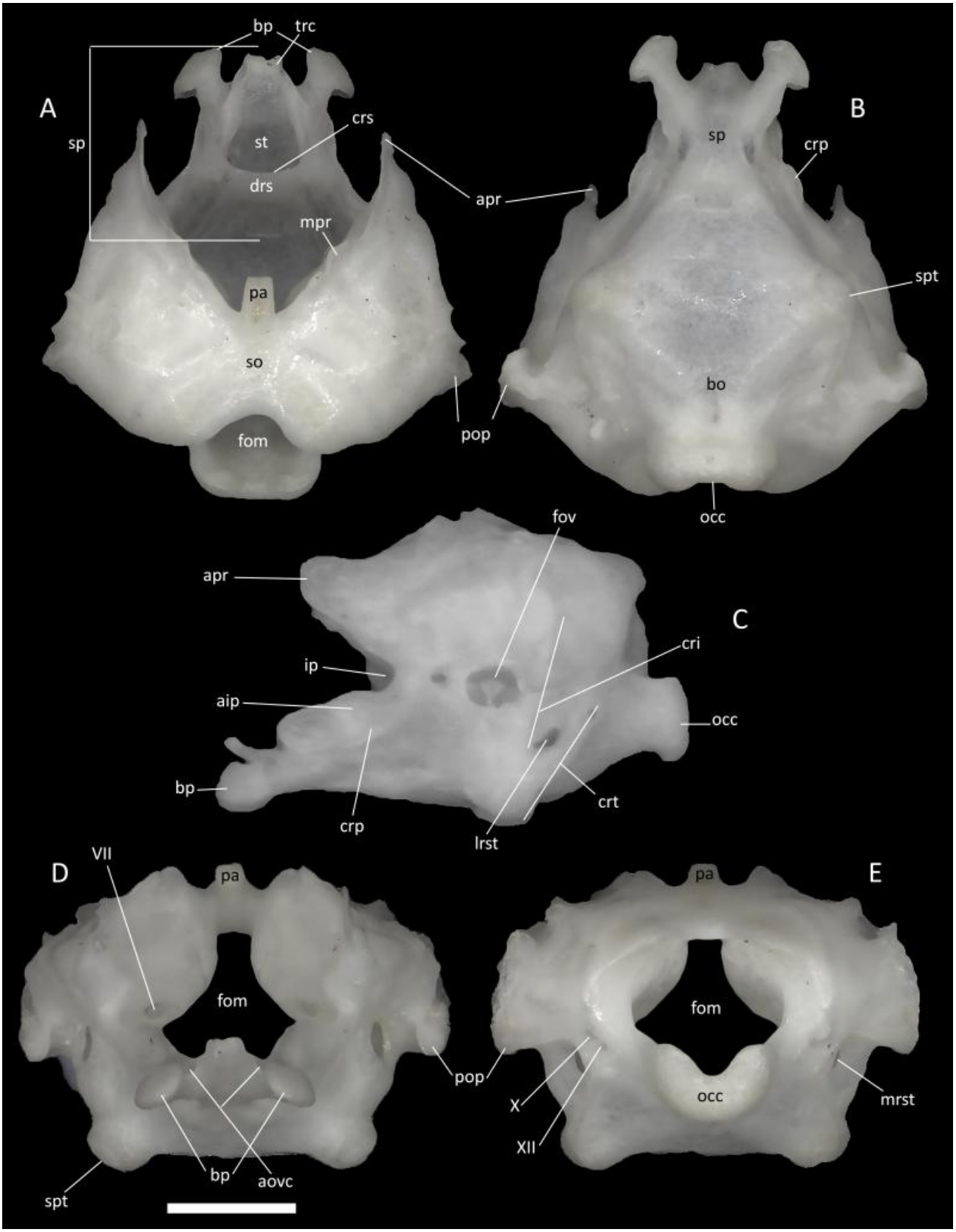

Figure 29. *Ophiomorus punctatissimus* MDHC 427, neurocranium. A: dorsal view; B: ventral view; C: left lateral view; D: anterior view; E: posterior view. Abbreviations: VII: foramen of the facial nerve; X: foramen for the vagus nerve; XII: foramen for the hypoglossal nerve; aip: anterior inferior process; aovc: anterior openings of the Vidian canals; apr: alar process; bo: basioccipital; bp: basipterygoid process; cri: crista interfenestralis; crp: crista prootica; crs: crista sellaris; crt: crista tuberalis; drs: dorsum sellae; fom: foramen

magnum; fov: foramen ovale; ip: incisura prootica; lrst: lateral opening recessus scalae tympani; mpr: marginal process; mrst: medial opening recessus scalae tympani; occ: occipital condyle; pa: processus ascendens; pop: paroccipital process; so: supraoccipital; sp: sphenoid; spt: sphenooccipital tubercle; st: sella turcica; trc: trabeculae cranii. Scale bar: 1 mm.

Fig. 30. *Ophiomorus punctatissimus* MCCI R775, endocast of the bony labyrinth. A: left lateral view, highlighted in the context of the skull; B: left lateral view, cropped from the skull. Abbreviations: amp: ampullae; asc: anterior semicircular canal; fo: foramen ovale; lsc: lateral semicircular canal; psc: posterior semicircular canal; ves: vestibule.

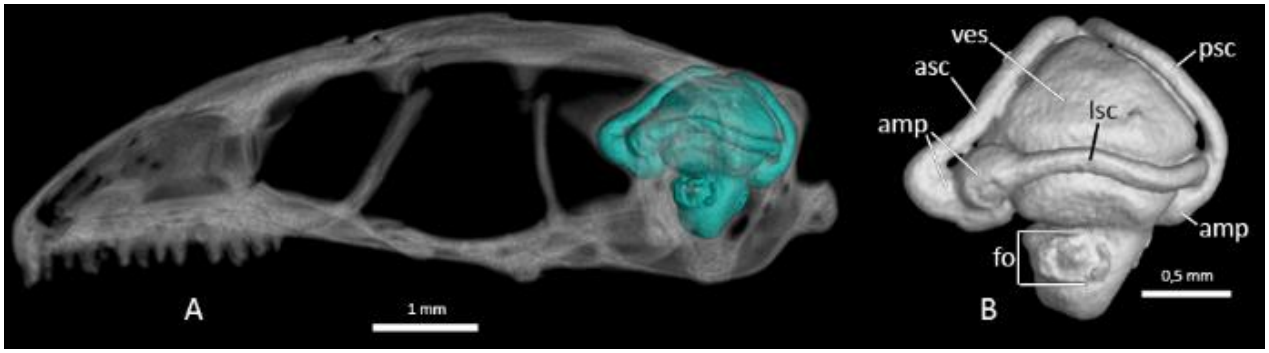

Fig. 31. *Ophiomorus punctatissimus* MCCI R952, endocast of the bony labyrinth. A: left lateral view, highlighted in the context of the skull; B: left lateral view, cropped from the skull. Abbreviations: amp: ampullae; asc: anterior semicircular canal; fo: foramen ovale; lsc: lateral semicircular canal; psc: posterior semicircular canal; ves: vestibule.

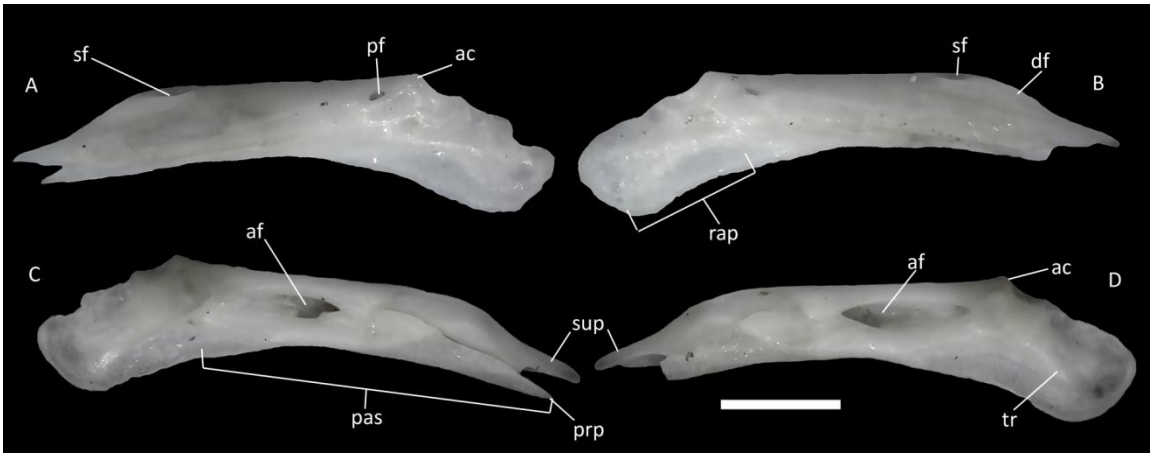

Figure 32. *Ophiomorus punctatissimus* MDHC 427, left (A, C) and right (B, D) articular complexes. A, B: lateral view; C, D: medial view. Abbreviations: ac: articular condyle; af: adductor fossa; df: dentary facet; pas: prearticular spine; pf: posterior surangular foramen; prp: prearticular process; rap: retroarticular process; sf: anterior surangular foramen; sup: surangular process; tr: tympanic ridge. Scale bar: 1 mm.

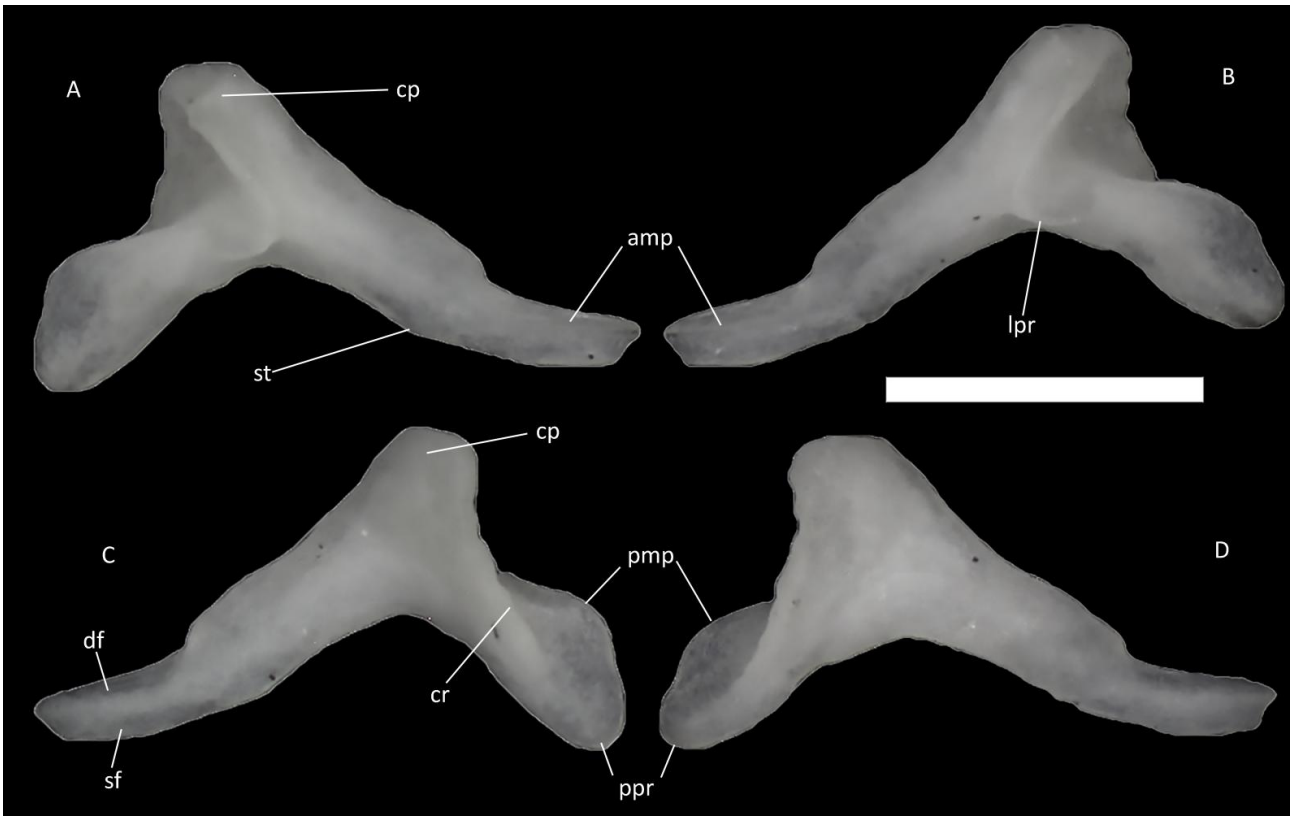

Figure 33. *Ophiomorus punctatissimus* MDHC 427, right (A, C) and left (B, D) coronoids. A, B: lateral view; C, D: medial view. Abbreviations: amp: anteromedial process; cp: coronoid process; cr: coronoid ridge; df: dentary facet; lpr: labial process; pmp: posteromedial process; ppr: posterior process; sf: splenial facet; st: step. Scale bar: 1 mm.

Figure 34. *Ophiomorus punctatissimus* MDHC 427, left splenial. A: medial view; B: lateral view. Abbreviations: aif: anterior inferior foramen; mf: anterior mylohyoid foramen. Scale bar: 1 mm.

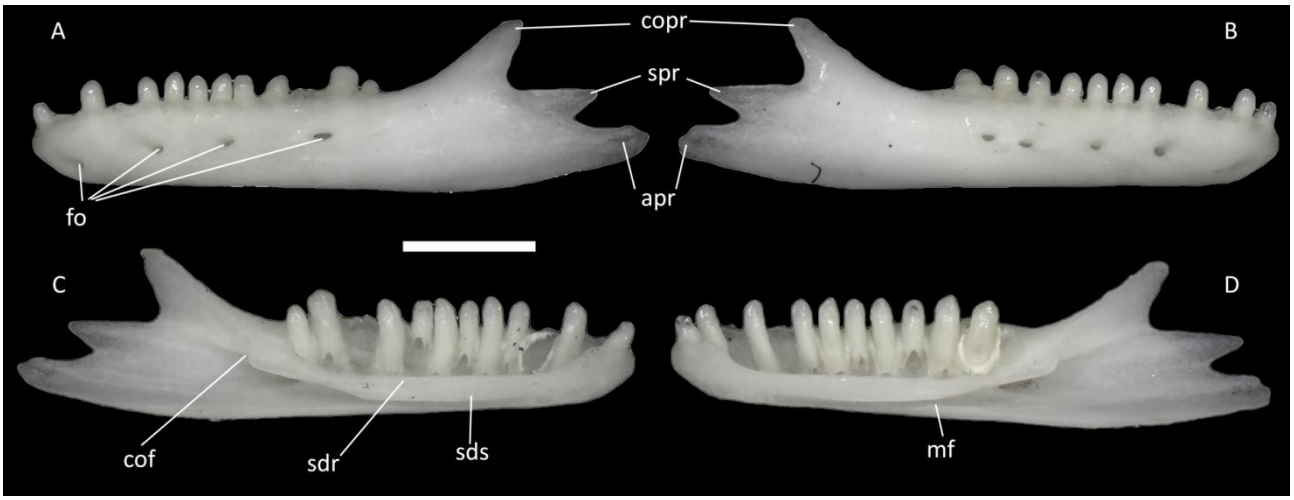

Figure 35. *Ophiomorus punctatissimus* MDHC 427, left (A, C) and right (B, D) dentaries. A, B: lateral view; C, D: medial view. Abbreviations: apr: angular process; cof: coronoid facet; copr: coronoid process; fo: foramina; mf: Meckelian fossa; sdr: subdental ridge; sds: subdental shelf; spr: surangular process. Scale bar: 1 mm.

Figure 36. *Ophiomorus punctatissimus* MDHC 427, left angular. A: lateral view; B: medial view. Abbreviations: apr: anterior process. Scale bar: 1 mm.

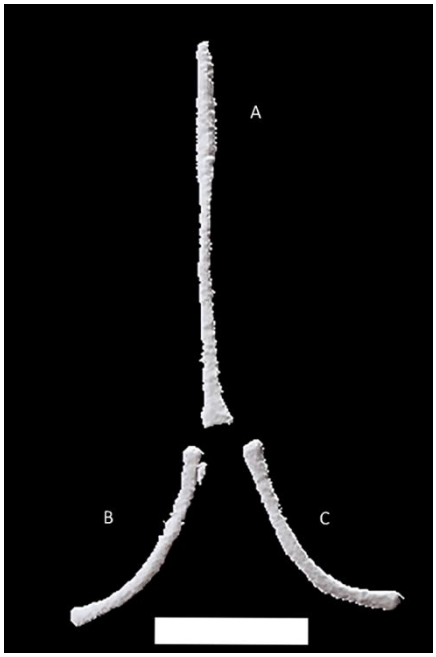

Figure 37. *Ophiomorus punctatissimus* MCCI R775, hyoid apparatus, comprised of basihyal (A), right (B) and left (C) first ceratobranchials in ventral view (visualized with Zbrush 4R8). Scale bar: 1 mm.

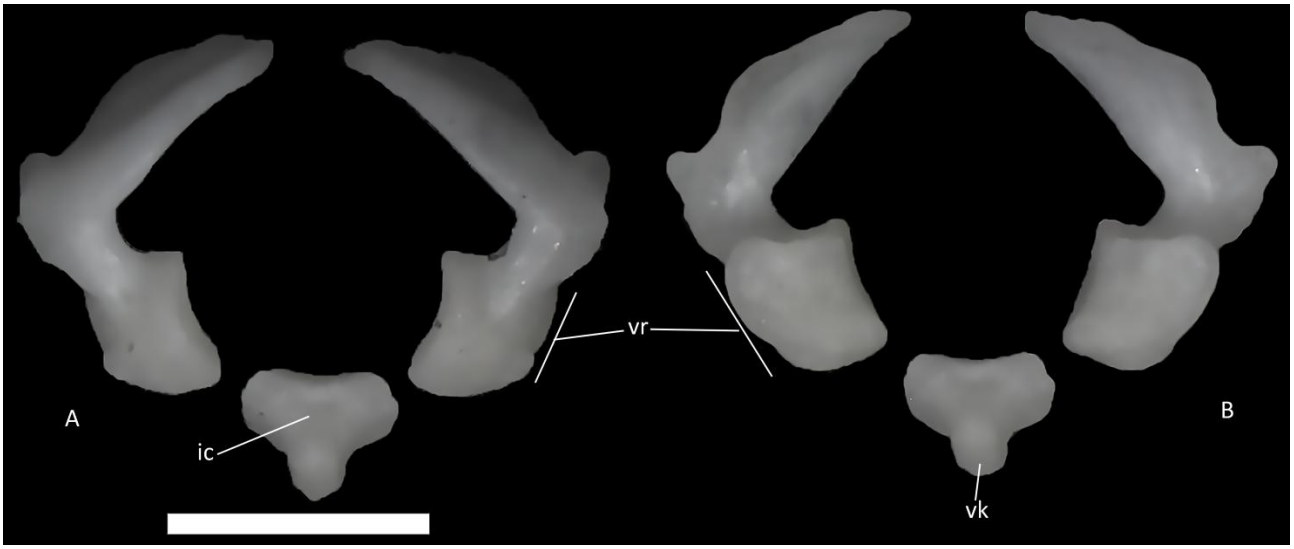

Figure 38. *Ophiomorus punctatissimus* MDHC 427, elements of the atlas. A: anterior view; B: posterior view. Abbreviations: ic: intercentrum; vr: ventral ramus; vk: ventral keel. Scale bar: 1 mm.

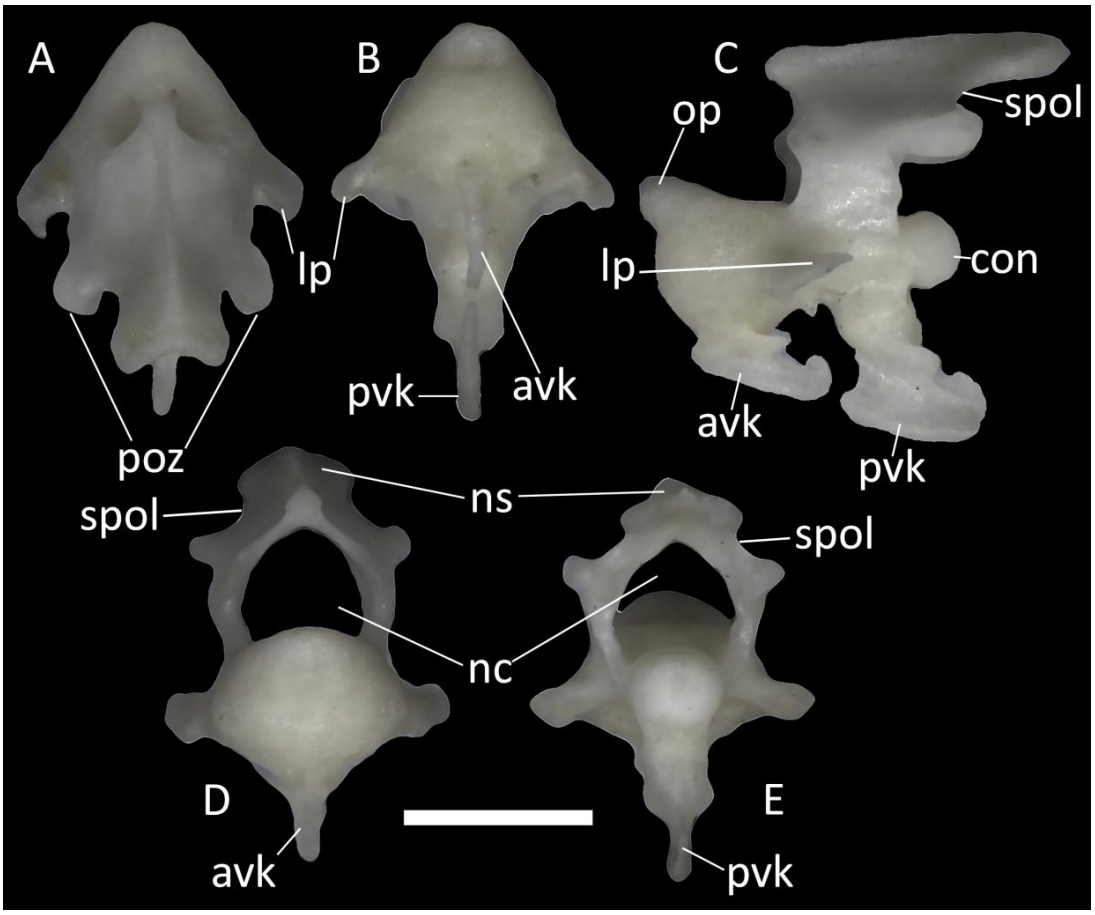

Figure 39. *Ophiomorus punctatissimus* MDHC 427, axis. A: dorsal view; B: ventral view; C: left lateral view; D: anterior view; E: posterior view. Abbreviations: avk: anterior ventral keel; con: condyle; lp: lateral process; nc: neural canal; ns: neural spine; op: odontoid process; poz: postzygapophyses; pvk: posterior ventral keel; spol: SPOL. Scale bar: 1 mm.

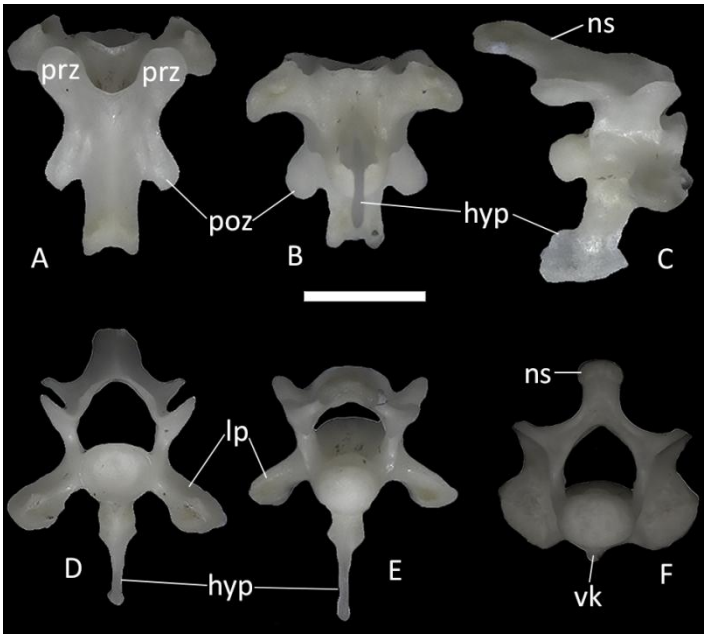

Figure 40. *Ophiomorus punctatissimus* MDHC 427, anterior postaxial cervical vertebra (A, B, C, D, E) and posterior postaxial cervical vertebra (F). A: dorsal view; B: ventral view; C: left lateral view; D: anterior view; E, F: posterior view. Abbreviations: hyp: hypapophysis; lp: lateral process; ns: neural spine; poz: postzygapophyses; prz: prezygapophyses; vk: ventral keel. Scale bar: 1 mm.

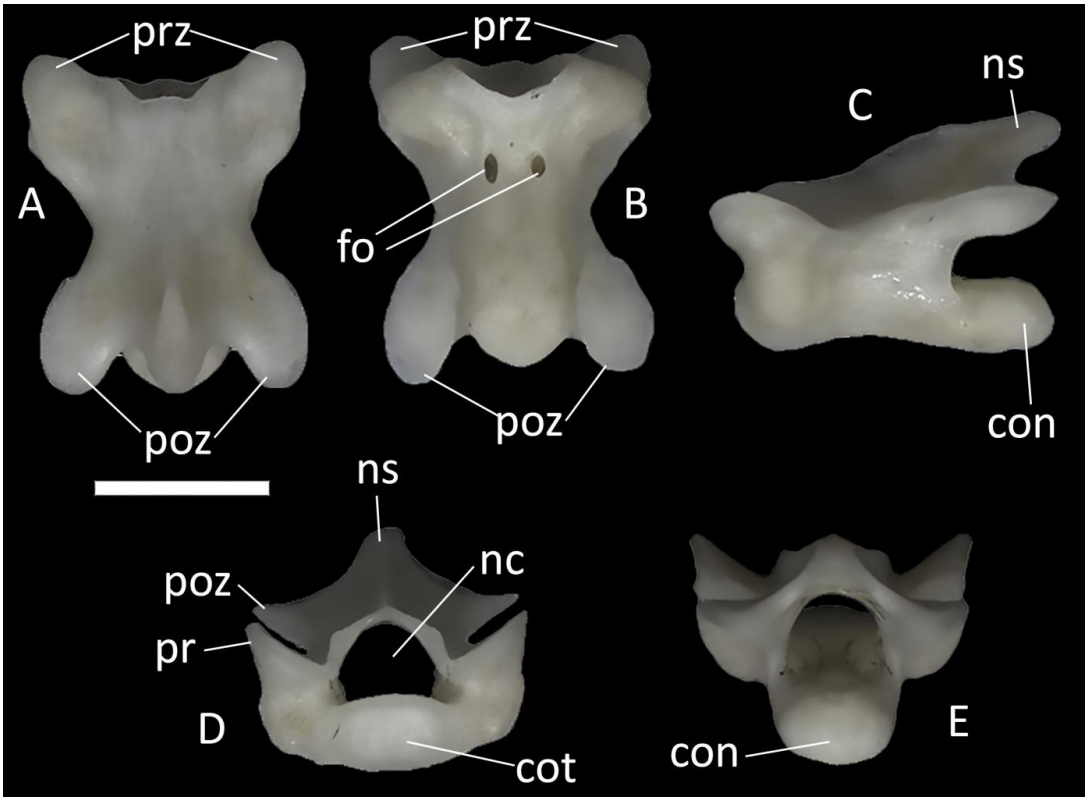

Figure 41. *Ophiomorus punctatissimus* MDHC 427, trunk vertebra. A: dorsal view; B: ventral view; C: left lateral view; D: anterior view; E: posterior view. Abbreviations: con: condyle; cot: cotyle; fo: foramina; nc: neural canal; ns: neural spine; poz: postzygapophyses; prz: prezygapophyses. Scale bar: 1 mm.

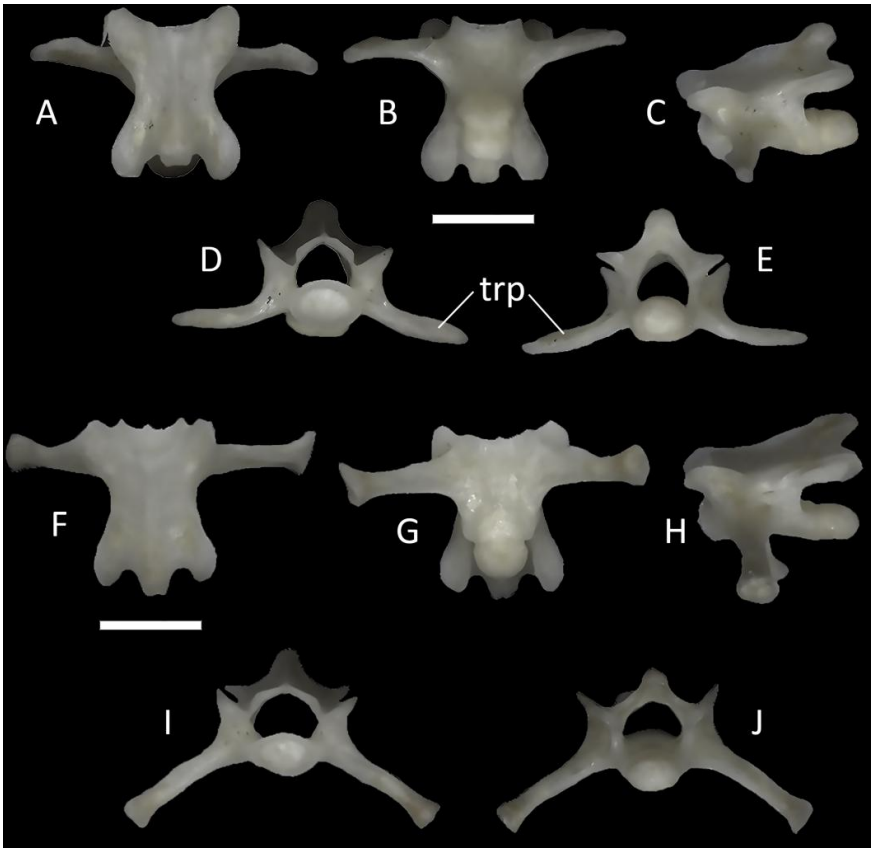

Figure 42. *Ophiomorus punctatissimus* MDHC 427, first sacral vertebra (A, B, C, D, E) and second sacral vertebra (F, G, H, I, J). A, F: dorsal view; B, G: ventral view; C, H: left lateral view; D, I: anterior view; E, J: posterior view. Abbreviations: trp: transverse process. Scale bar: 1 mm.

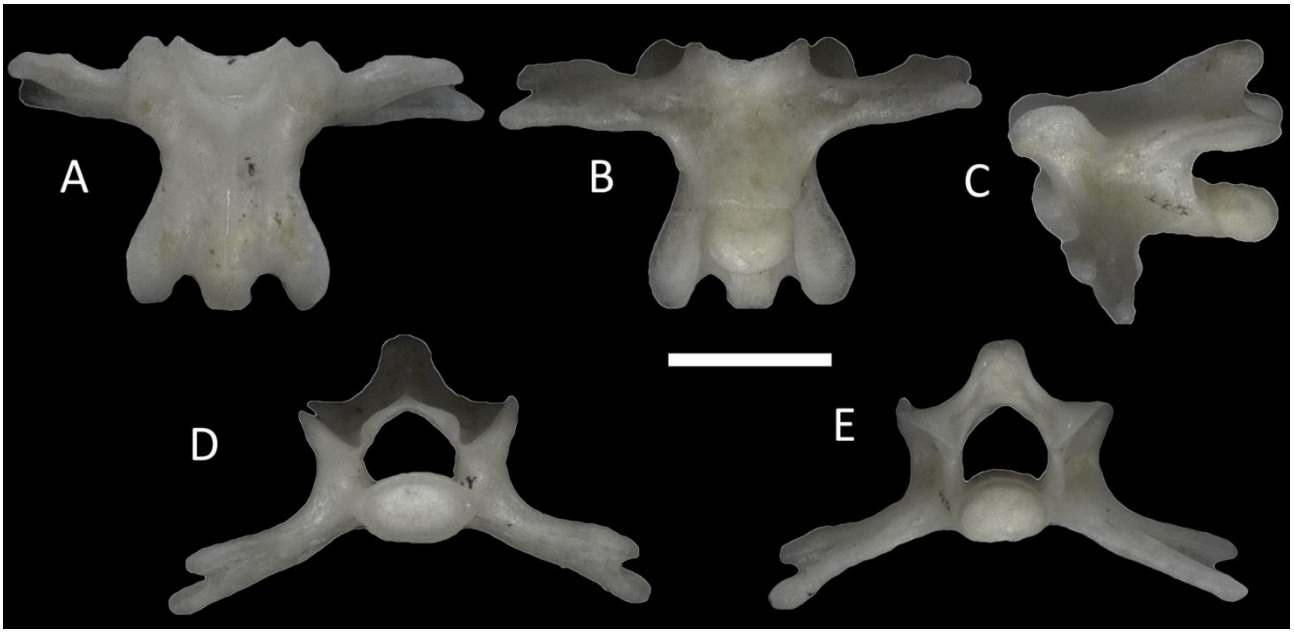

Figure 43. *Ophiomorus punctatissimus* MDHC 427, non-autotomic caudal vertebra. A: dorsal view; B: ventral view; C: left lateral view; D: anterior view; E: posterior view. Scale bar: 1 mm.

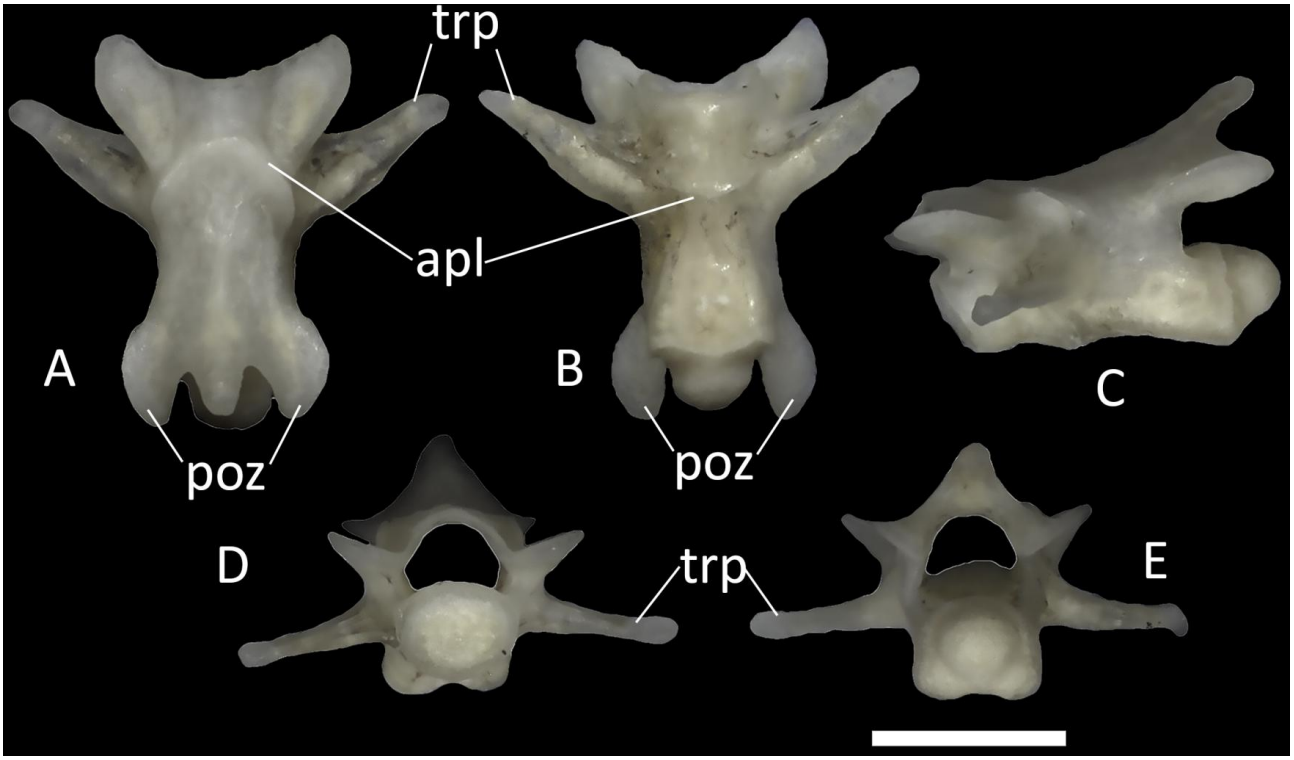

Figure 44. *Ophiomorus punctatissimus* MDHC 427, autotomic caudal vertebra. A: dorsal view; B: ventral view; C: left lateral view; D: anterior view; E: posterior view. Abbreviations: apl: autotomy plane; poz: postzygapophyses; trp: transverse process. Scale bar: 1 mm.

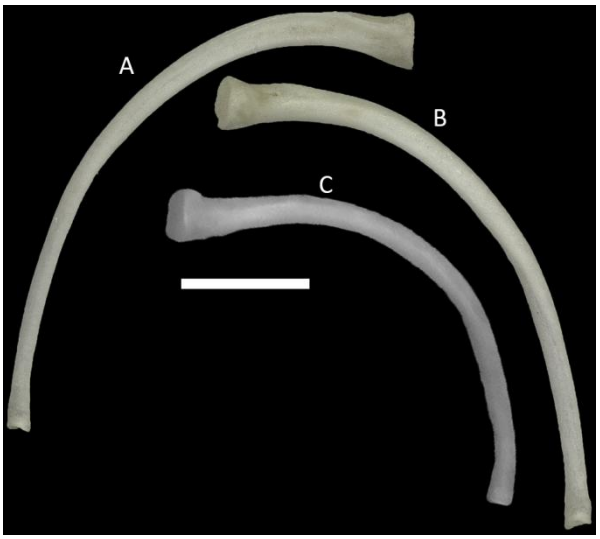

Figure 45. *Ophiomorus punctatissimus* MDHC 427, thoracic ribs. A: anterior view; B, C: posterior view. Scale bar: 1 mm.

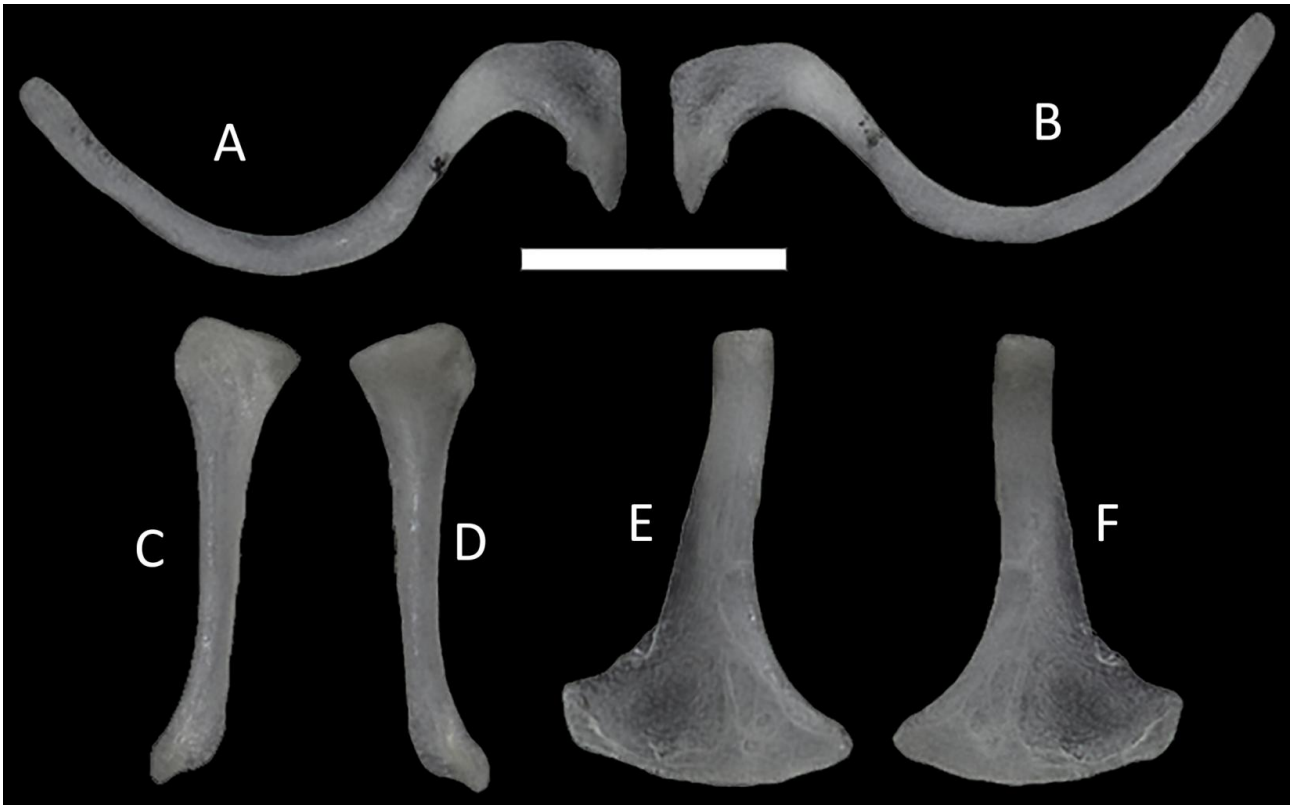

Figure 46. *Ophiomorus punctatissimus* MDHC 427 left clavicle (A, B), right scapula (C, D) and right coracoid (E, F). A: dorsal view; B: ventral view C, E: lateral view; D, F: medial view. Scale bar: 1 mm.

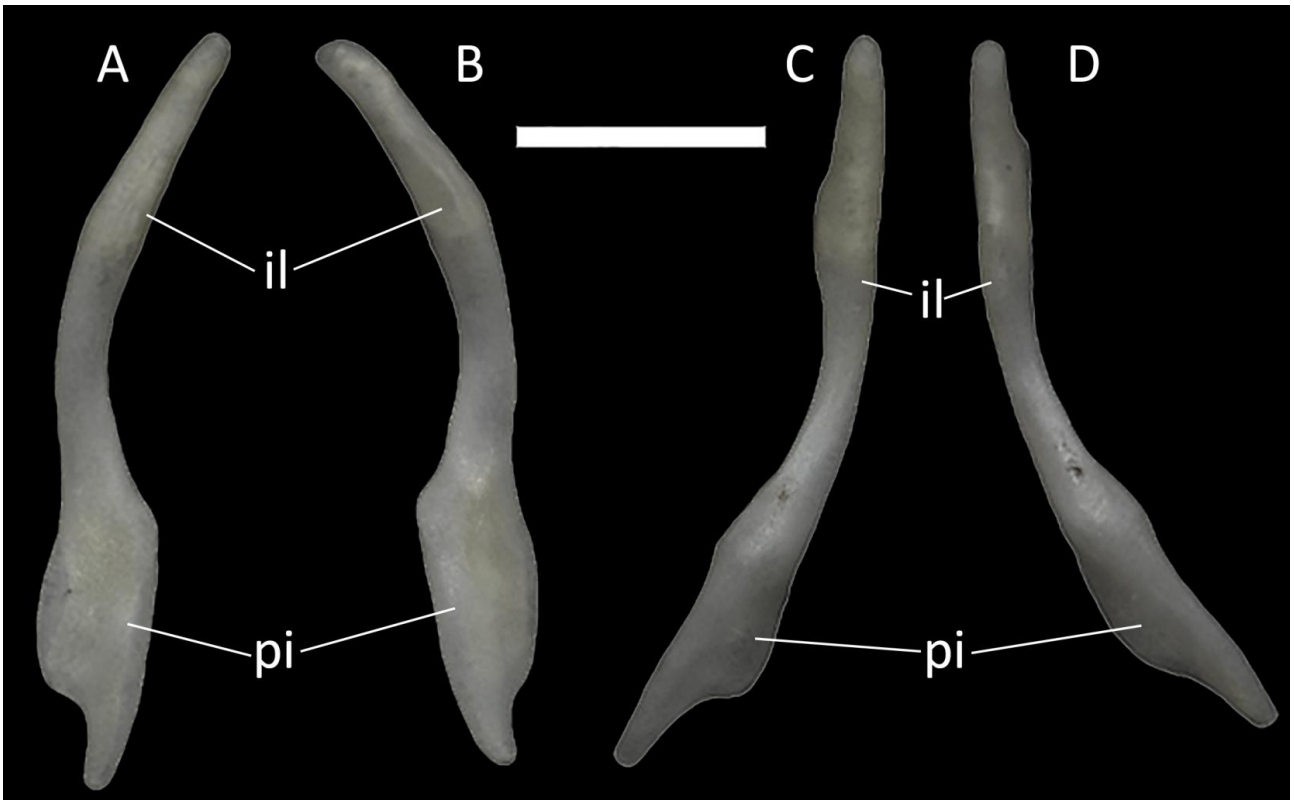

Figure 47. *Ophiomorus punctatissimus* MDHC 427, right (A, C) and left (B, D) pelvic elements. A, B: anterior view; C, D: posterior view. Abbreviations: il: ilium; pi: puboischium. Scale bar: 1 mm.